



**Iron(II)  $\beta$ -ketiminate complexes as mediators of controlled radical polymerisation**

Journal:	<i>Dalton Transactions</i>
Manuscript ID	DT-ART-03-2016-001208.R1
Article Type:	Paper
Date Submitted by the Author:	28-Apr-2016
Complete List of Authors:	Lake, Benjamin; University of Edinburgh, School of Chemistry Shaver, Michael; University of Edinburgh, School of Chemistry



## Iron(II) $\beta$ -ketiminate complexes as mediators of controlled radical polymerisation†

Received 00th January 20xx,  
Accepted 00th January 20xx

Benjamin R. M. Lake<sup>a</sup> and Michael. P. Shaver\*<sup>a</sup>

DOI: 10.1039/x0xx00000x

www.rsc.org/

A series of tridentate, ONO- and ONN-chelating  $\beta$ -ketiminate ligands were synthesised *via* condensation reactions, and complexed with iron(II) using  $[\text{Fe}(\text{N}(\text{SiMe}_3)_2)_2\text{THF}]$ . The complexation reactions proceeded in high yields to generate novel, monomeric, tetracoordinate iron(II) complexes, each bearing a *bis*(trimethylsilyl)amide ligand, as confirmed by X-ray crystallography. These complexes were amenable to further reaction (protonolysis) with alcohols and phenols, generating alkoxide/phenolate-containing complexes that were dimeric in the solid state. All complexes synthesised were screened as potential mediators of the controlled radical polymerisation (CRP) of styrene and methyl methacrylate under both atom transfer radical polymerisation (ATRP) and organometallic mediated radical polymerisation (OMRP) conditions. Whilst all of the complexes were relatively poor ATRP mediators under the conditions used here, regardless of monomer choice, dispersities ( $\bar{M}_w/\bar{M}_n$ ) as low as 1.58 for styrene and 1.23 for methyl methacrylate polymerisation under OMRP conditions could be achieved. The better performance in methacrylate polymerisation suggests the formation of a stronger metal-carbon bond in these systems. In particular, the use of a  $\beta$ -ketiminate ligand functionalised with an *N,N*-dimethylethylene pendant arm and a 2,6-diphenylphenolate ligand affords, to our knowledge, the best Fe-based mediator of methacrylate OMRP described in the literature.

### Introduction

The application of iron compounds as catalysts in organic chemistry is a vibrant area of research.<sup>1</sup> This is due, in part, to the low cost of iron, its high crustal abundance, and its biocompatibility. Furthermore, the ability of iron to adopt a range of oxidation states (-2 to +5) and spin-states allows it to display remarkably variable reactivity, thus allowing it to participate in a wide range of chemical reactions. Indeed, soon after the pioneering initial reports by the groups of Matyjaszewski<sup>2</sup> and Sawamoto<sup>3</sup> on the controlled radical polymerisation (CRP) of alkene monomers, the first reports of the use of iron complexes as mediators of this important reaction began to appear.<sup>4</sup> The use of iron complexes as mediators of CRP has now grown so considerably, that a number of reviews covering this thriving field have been recently published.<sup>5</sup>

As part of our continuing studies on utilising new iron-based mediators for CRP<sup>6</sup> and understanding the underlying mechanisms by which these complexes impart control over polymerisation reactions,<sup>7</sup> we sought to develop a new series of iron complexes based on the  $\beta$ -ketiminate ligand scaffold. Iron- $\beta$ -ketiminate complexes have been scarcely used as mediators of CRP,<sup>5a, 5c</sup> with only one report to the best of our knowledge published to date.<sup>8</sup> We specifically chose  $\beta$ -ketiminates to support our iron complexes, due to the ease with which these ligands are synthesised and the inexpensive

starting materials required to make them, both of which would be especially attractive features for use at production scale.<sup>9</sup> Furthermore, the electronic and steric characteristics can be controlled by tuning the  $\beta$ -ketiminate scaffold, including through the introduction of additional donors. This ability to shape the coordination sphere could be especially important as we pursue systems that can reversibly trap radicals *via* the formation of a new metal-carbon bond.

In this report, we detail the synthesis of  $\alpha,\beta$ -unsaturated- $\beta$ -ketoamines bearing pendant amine, ether and pyridyl donors. The reaction of these compounds with the iron-containing precursor  $[\text{Fe}(\text{N}(\text{SiMe}_3)_2)_2\text{THF}]$  produced a series of four-coordinate complexes, with bound *bis*(trimethylsilyl)amide donors. A second family of catalysts was generated through protonolysis of these compounds with benzyl alcohol or 2,6-diphenylphenol, yielding dimeric (in the solid state) iron(II) complexes bearing alkoxide or phenolate ligands. All of the iron complexes synthesised were examined as mediators of CRP under both atom transfer radical polymerisation (ATRP, alkyl halide initiator) and organometallic mediated radical polymerisation (OMRP, azo initiator) conditions.

By using iron(II) rather than the more stable iron(III) complexes, we are able to separate out the halogen and organometallic mechanisms and draw conclusions about the role of both ATRP and OMRP equilibria (*vide infra*) in imparting control over the polymerisation reactions described herein. The information gained during the course of these studies is additionally of potential relevance to all metal mediated CRP

<sup>a</sup> EaStCHEM School of Chemistry, University of Edinburgh, Edinburgh, EH9 1JJ, UK.

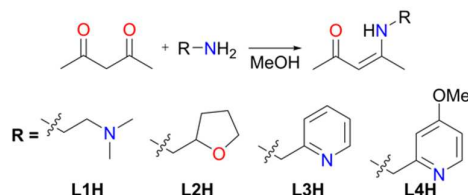
†Electronic Supplementary Information (ESI) available: GPC data, <sup>1</sup>H NMR spectra and single crystal x-ray diffraction data. CCDC 1470307-1470310, 1470323-1470324 and 1470383-1470385. For ESI and crystallographic data in CIF format see DOI: 10.1039/x0xx00000x

reactions, and is helping to guide our development of effective iron-based mediators.

## Results and discussion

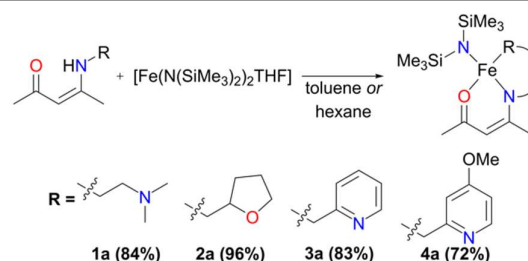
### Synthesis and Characterisation

The synthesis of  $\alpha,\beta$ -unsaturated- $\beta$ -ketoamines, precursors to  $\beta$ -ketiminates, bearing pendant donor functionalities was achieved *via* the condensation of acetylacetone and the appropriate primary amine at reflux (Scheme 1). Contrary to previously published reports,<sup>10</sup> we found that the reactions proceeded efficiently in methanol without the need for an acid catalyst. The ligand precursors **L1H** and **L2H** were obtained as pale yellow oils following purification by vacuum distillation, while **L3H** and **L4H** could be obtained as colourless crystalline solids by recrystallisation. All four  $\alpha,\beta$ -unsaturated- $\beta$ -ketoamines display broad singlet resonances between 10.77 - 11.26 ppm ( $\text{CDCl}_3$ ), characteristic of the hydrogen-bonded amine proton.<sup>11</sup> Ligand precursors **L3H** and **L4H** also each show a doublet resonance ( $J \approx 6.5$  Hz) at 4.57 and 4.52 ppm ( $\text{CDCl}_3$ ), respectively, corresponding to the picolyl- $\text{CH}_2$  protons coupling to the amine proton.



Scheme 1 Synthesis of **L1H** – **L4H**

Previous publications have reported the synthesis of transition metal complexes bearing donor-tethered  $\beta$ -ketiminates using various strategies, including by reaction of the ligand precursor and metal salt in the presence of a base<sup>10a</sup> and without a base,<sup>12</sup> by reaction of the ligand precursor with a highly basic metal starting reagent<sup>13</sup> and by transmetalation from an alkali metal- $\beta$ -ketimate complex.<sup>10c, 14</sup> We decided to use a simple strategy and form our desired  $\text{Fe}^{\text{II}}(\text{L})(\text{N}(\text{SiMe}_3)_2)$ -type complexes in a one-pot reaction using  $[\text{Fe}(\text{N}(\text{SiMe}_3)_2)_2\text{TfH}]$  as the basic metalating reagent. Indeed, reaction of the  $\alpha,\beta$ -unsaturated- $\beta$ -ketoamines, **L1H** – **L4H**, with an equimolar amount of  $[\text{Fe}(\text{N}(\text{SiMe}_3)_2)_2\text{TfH}]$  in hexane or toluene led to the formation of green-yellow solutions/suspensions, from which, highly oxygen and moisture-sensitive solids could be obtained upon work-up (Scheme 2). The products (**1a** – **4a**) were obtained in good yields (> 72%) and isolated as green crystalline solids. Characterisation of **1a** – **4a** by  $^1\text{H}$  NMR spectroscopy revealed paramagnetically-shifted spectra, with a series of broad resonances between approximately -60 and 180 ppm present in each spectrum (see Supporting Information). The solution magnetic moments of these complexes were suggestive of  $d^6$  high-spin electron configurations at ambient temperature, with calculated values (4.9 – 5.4  $\mu_B$ ) congruent with the spin-



Scheme 2 Synthesis of **1a** – **4a**

only magnetic moment of a high-spin iron(II) centre (4.90  $\mu_B$ ). Single crystals of all four complexes (**1a** – **4a**) suitable for X-ray diffraction analysis could be obtained, either directly from the bulk material, or by cooling a saturated *n*-hexane solution of the product to -35°C. The molecular structures of complexes **1a** – **4a** are provided in Figures 1 and 2 along with selected bond lengths and angles. All four complexes have crystallised as monomeric, four-coordinate species, with the coordination sphere of each comprising the N,O-donors of the  $\beta$ -ketimate backbone, the heteroatom of the tethered donor and the N atom of a *bis*(trimethylsilyl)amide. The coordination geometries about all four iron(II) centres (**1a** – **4a**) can be described as distorted seesaw according to the four-

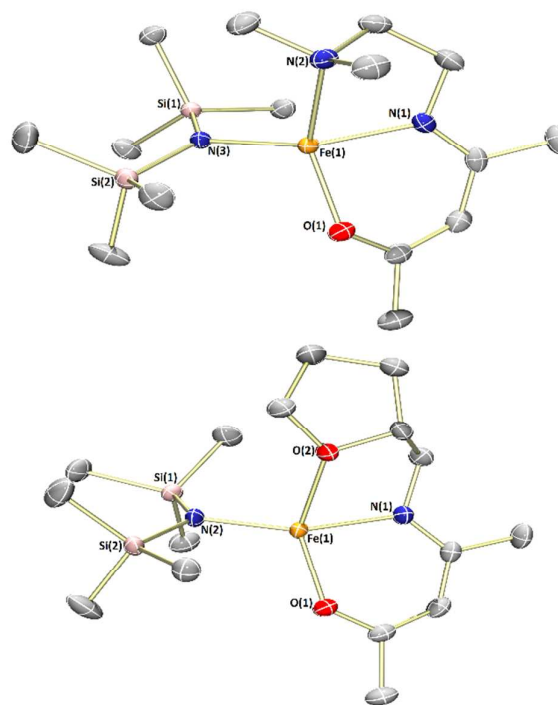
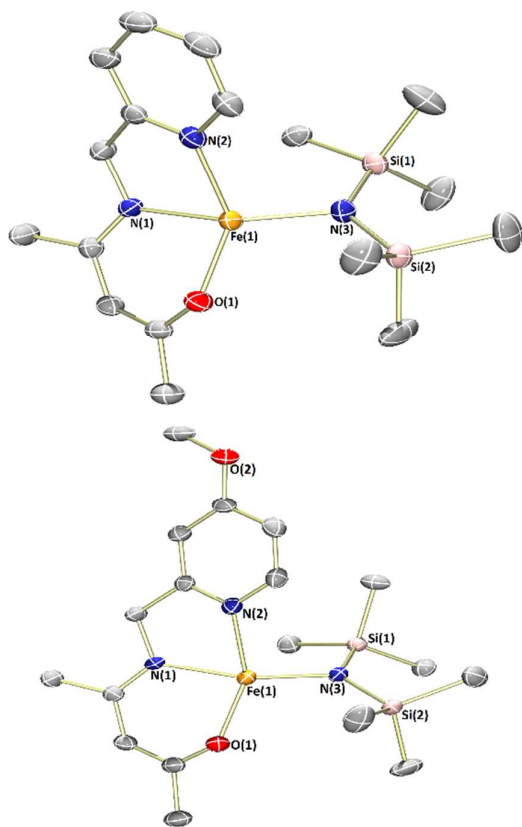


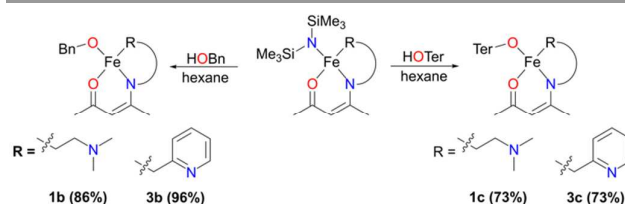
Figure 1 Molecular structures of **1a** (top) and **2a** (bottom) with ellipsoids set at the 50% probability level. Hydrogen atoms have been omitted for clarity. Selected bond lengths (Å) and angles (°): **1a** - Fe1-O1 1.9601(11), Fe1-N1 2.0409(13), Fe1-N2 2.2342(13), Fe1-N3 1.9596(13), O1-Fe1-N2 134.54(5), O1-Fe1-N1 90.24(5), N3-Fe1-O1 110.48(5), N3-Fe1-N2 105.08(5), N3-Fe1-N1 140.40(5), N1-Fe1-N2 79.40(5). **2a** - Fe1-O1 1.9614(9), Fe1-N1 2.0559(10), Fe1-O2 2.1418(9), Fe1-N2 1.9472(9), O1-Fe1-O2 133.40(4), O1-Fe1-N1 89.56(4), N1-Fe1-O2 76.66(4), N2-Fe1-O1 113.98(4), N2-Fe1-O2 98.99(4), N2-Fe1-N1 148.22(4)

coordinate geometry index proposed by Houser in the pages of this journal,<sup>15</sup> with  $\tau_4$  values of 0.60, 0.56, 0.57 and 0.54 respectively. The coordination geometries can alternatively be described using Alvarez's system,<sup>16</sup> which suggests a tendency towards an intermediate (spread) geometry. This geometry is extremely rare indeed for  $d^6$  metal ions,<sup>16a</sup> and it is likely that the unusual coordination geometry is imposed by a combination of the conformational requirements of the relatively rigid tridentate  $\beta$ -ketiminate ligand, and the extreme steric bulk imparted by the *bis*(trimethylsilyl)amide donor. The bond metrics of **1a** – **4a** are comparable to those of the iron(II)- $\beta$ -ketiminates (though most of these are iron(II)-*bis*- $\beta$ -ketiminate complexes) reported in the literature so far,<sup>8, 11, 17</sup> with  $O_{ketiminate}$ -Fe bond lengths of 1.96 Å and  $N_{ketiminate}$ -Fe bond lengths of between 2.04 – 2.06 Å. The  $N_{hmds}$ -Fe bond lengths of 1.95 – 1.96 Å are slightly longer than those of the three-coordinate starting material (1.92 Å),  $[Fe(N(SiMe_3)_2)THF]$ ,<sup>18</sup> but compare reasonably well with the  $N_{hmds}$ -Fe<sup>II</sup> bond lengths in other reported four-coordinate complexes containing a coordinated *bis*(trimethylsilyl)amide.<sup>19</sup>



**Figure 2** Molecular structures of **3a** (top) and **4a** (bottom) with ellipsoids set at the 50% probability level. Hydrogen atoms have been omitted for clarity. Selected bond lengths (Å) and angles (°): **3a** - Fe1-O1 1.9599(14), Fe1-N1 2.0598(16), Fe1-N2 2.1443(17), Fe1-N3 1.9574(17), O1-Fe1-N1 88.95(6), O1-Fe1-N2 132.28(6), N1-Fe1-N2 77.67(7), N3-Fe1-O1 112.75(7), N3-Fe1-N1 147.36(7), N3-Fe1-N2 101.77(7). **4a** - Fe1-O1 1.9638(13), Fe1-N1 2.0601(14), Fe1-N2 2.1430(16), Fe1-N3 1.9547(14), O1-Fe1-N1 89.02(6), O1-Fe1-N2 140.71(6), N1-Fe1-N2 77.97(6), N3-Fe1-O1 111.83(6), N3-Fe1-N1 143.53(6), N3-Fe1-N2 99.82(6)

The *bis*(trimethylsilyl)amide-containing complexes **1a** and **3a** were amenable to protonolysis reactions (complexes **2a** and **4a** were not examined). Reaction of either of these two complexes with a hexane solution of benzyl alcohol led to an immediate and distinct colour change from green-yellow to red or orange. After a simple work-up, the products **1b** and **3b** were isolated as orange and red solids respectively (Scheme 3).



**Scheme 3** Synthesis of complexes **1b**, **3b**, **1c** and **3c**

Analysis of the products by <sup>1</sup>H NMR spectroscopy again revealed a series of paramagnetically-shifted resonances, with solution magnetic moment data ( $\mu_{eff} = 5.4$  and  $5.2 \mu_B$ , respectively) indicative of  $d^6$  high-spin electron configurations. Single crystals of complex **1b** suitable for X-ray diffraction analysis were obtained on cooling of a saturated *n*-hexane solution from reflux (Figure 3). The solid-state structure of **1b** reveals a dimer, with  $(\mu^2-OBn)_2$  bridging the two iron(II) centres. The two halves of the dimer are related to each other through a crystallographic inversion centre, located in the centre of the  $Fe_2O_2$  rhombus, with each five-coordinate iron(II) possessing a coordination geometry best described as square pyramidal. Single crystals of complex **3b**, obtained from a dilute toluene/*n*-hexane solution stored at  $-35^\circ C$ , show that this complex is isostructural with **1b**.

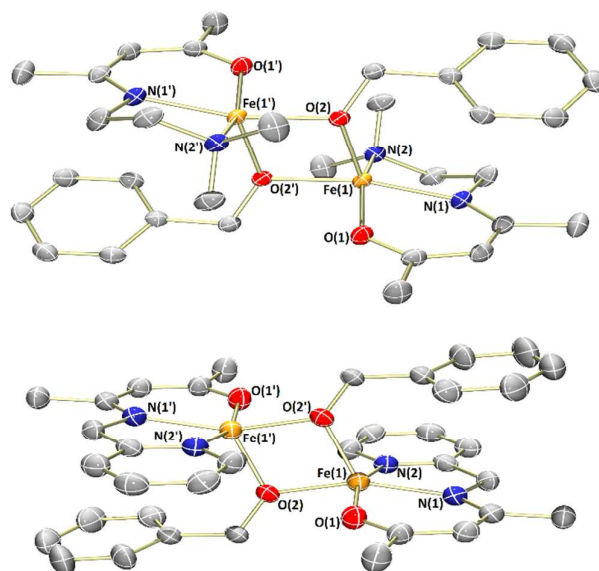


**Figure 3** Molecular structures of **1b** (top) and **3b** (bottom) with ellipsoids set at the 50% probability level. Hydrogen atoms have been omitted for clarity. Selected bond lengths (Å): **1b** - Fe1-O1 2.0223(10), Fe1-O2 2.0354(9), Fe1-O2' 2.0436(9), Fe1-N1 2.0908(12), Fe1-N2 2.2864(12). **3b** - Fe1-O1 1.994(4), Fe1-O2 2.047(4), Fe1-O2' 2.061(4), Fe1-N1 2.102(4), Fe1-N2 2.171(5).

As an electronic and steric contrast between the bulky amide-containing complexes **1a** – **4a**, and the relatively non-bulky alkoxide-containing complexes **1b** and **3b**, we decided to synthesise bulky phenoxide-containing complexes of iron(II) bearing our tridentate  $\beta$ -ketiminate ligands. Terphenolate was chosen in this case, as it has been shown to support iron in the +2 and +3 oxidation states and in a number of different coordination geometries.<sup>20</sup> Furthermore, it has been shown that the steric bulk provided by terphenolate ligands can enhance reactivity by protecting a coordination site at the metal centre.<sup>21</sup> Similarly to the synthesis of benzyl alkoxide-substituted complexes **1b** and **3b**, reaction of parent complexes **1a** and **3a** with 2,6-diphenylphenol (HOTer) led to immediate colour changes, and isolation of yellow/orange solids following work-up (Scheme 3). The terphenolate-substituted complexes **1c** and **3c** were obtained in good yields (73%), and could be fully characterised, including by single crystal X-ray diffraction analysis (Figure 4). The solid-state structure of **1c** again reveals a dimer, with the crystallographic asymmetric unit containing two structurally similar molecules of dimer and two molecules of solvent (see Supporting Information), though both the solvent and one dimer have been omitted for clarity's sake in Figure 4. Complex **1c** contains iron(II) centres bridged by the two oxygen atoms of the two substituted  $\beta$ -ketiminates, with the terphenolate ligands bound in a terminal fashion. The central Fe<sub>2</sub>O<sub>2</sub> rhombus of

both dimers is noticeably puckered, while those of complexes **1b** and **3b** are planar, which presumably helps alleviate steric clashing between adjacent terphenolate aromatic rings. The four iron(II) centres contained within the two dimers of the asymmetric unit possess a range of coordination geometries, from slightly distorted square pyramidal to intermediate. Given the bridging nature of the  $\beta$ -ketiminate oxygen atoms, it is not surprising that the O<sub>ketiminate</sub>-Fe bond distances are typically somewhat longer than those found in either **1a** or **1b**, with lengths of between 2.05 – 2.18 Å. In contrast to **1c**, the two iron(II) centres of complex **3c** are bridged by an oxygen atom of one of the  $\beta$ -ketiminates and an oxygen atom of one of the terphenolates. The reason for this bridging mode is somewhat unclear, though maximising intramolecular  $\pi$ - $\pi$  stacking interactions between the terphenolate and pyridyl rings could be a contributory factor.

### Controlled Radical Polymerisation

The two main equilibria by which metal-mediated CRP proceeds are ATRP and OMRP (Scheme 4).<sup>22</sup> ATRP involves the reversible transfer of a halogen between a metal centre and propagating radical, while metal-carbon bonds are reversibly formed in OMRP. ATRP and OMRP equilibria are able to operate simultaneously *via* the same iron(II) species when reactions are performed under ATRP conditions (alkyl halide initiator), though an OMRP-only regime can be accessed in the absence of alkyl halide (using an azo initiator). For reactions set-up under ATRP conditions, the degree of involvement of an OMRP mechanism is highly dependent on the metal centre, ligand environment and monomer involved.<sup>5b, 7a, 7b, 7d, 9, 23</sup>

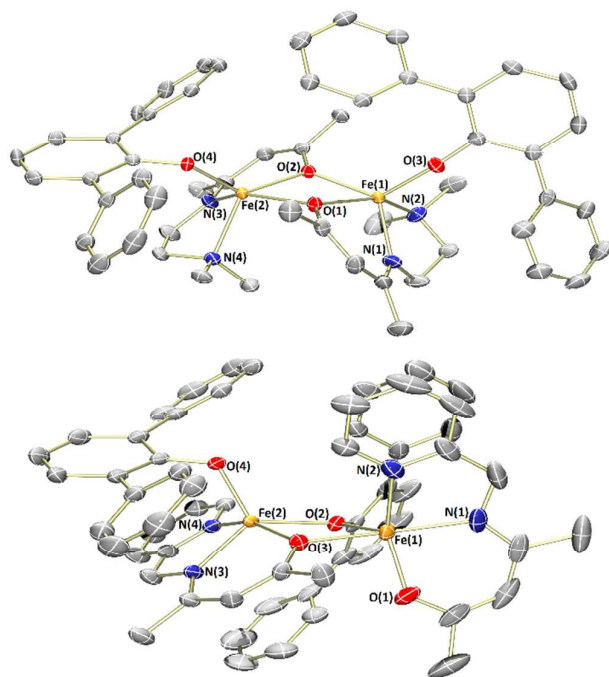
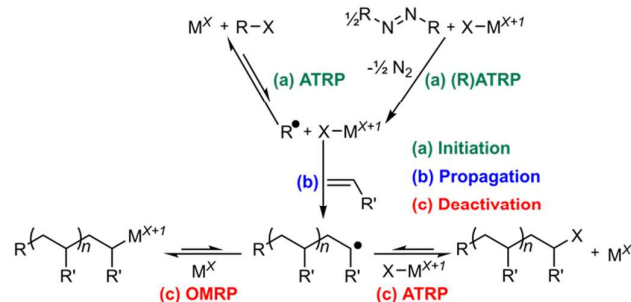


**Figure 4** Molecular structures of **1c** (top) and **3c** (bottom) with ellipsoids set at the 50% probability level. Hydrogen atoms and co-crystallised solvent have been omitted for clarity. Selected bond lengths (Å): **1c** - Fe1-O1 2.097(2), Fe1-O2 2.100(2), Fe1-O3 1.894(2), Fe1-N1 2.109(3), Fe1-N2 2.248(3), Fe2-O1 2.176(2), Fe2-O2 2.049(2), Fe2-O4 1.942(2), Fe2-N3 2.126(3), Fe2-N4 2.228(3). **3c** - Fe1-O1 1.985(2), Fe1-O2 2.045(2), Fe1-O3 2.120(2), Fe1-N1 2.084(3), Fe1-N2 2.133(3), Fe2-O2 2.107(2), Fe2-O3 2.077(2), Fe2-O4 1.970(2), Fe2-N3 2.080(3), Fe2-N4 2.154(3)



**Scheme 4** Equilibria implicated in CRP<sup>6b</sup>

**Atom Transfer Radical Polymerisation (ATRP).** All complexes were screened as mediators of the atom transfer radical polymerisation (ATRP) of styrene and methyl methacrylate (MMA), under the same reaction conditions we have previously described.<sup>7d</sup> The screening data obtained from the ATRP of styrene and MMA using our iron(II)- $\beta$ -ketiminate complexes as mediators and (1-chloroethyl)benzene (1-PECl) as the initiator is provided in Tables S1 and S2 in the Supporting Information section. All of the complexes are poor mediators of styrene ATRP, with broad dispersities ( $\bar{D} > 1.66$ ) and number average molecular weights ( $M_n$ ) far in excess of the theoretically predicted values ( $M_{n,th}$ ) derived from percentage conversion. The data obtained from the ATRP of

MMA under identical conditions to those used for styrene polymerisation suggests that almost all of the iron(II)- $\beta$ -ketiminate complexes screened are poor mediators of MMA ATRP, with picolyl-tethered complexes **3a** and **3b** offering a moderate degree of control ( $\bar{D}$  = 1.45 and 1.41 respectively). In all cases however, molecular weights are in excess of theoretical values predicted using the initial concentration of the initiator. This suggests inefficient initiation, and the potential of rapid radical termination reactions. However, initiators which produce MMA-type primary radicals and which have an ATRP equilibrium constant at least the same as that of propagating MMA-type radicals (e.g. ECPA and EBPA) might be expected to lead to a more efficient initiation process than when using 1-PECl. Therefore, while initial screening in related systems showed no significant impact on the nature of initiator, further ATRP studies with the use of initiators like ECPA could be performed if ATRP mediation of MMA is needed. Also if the Fe-Cl bonds are too strong, radical concentration would remain high, concomitantly increasing dispersity and molecular weight.

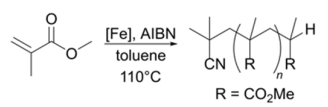
**Organometallic Mediated Radical Polymerisation (OMRP).** Compared with (R)ATRP, the use of iron complexes as mediators of OMRP has received much less attention, with few examples of the use of iron(II) complexes in pure OMRP processes.<sup>5a,5c,7d,23a,24</sup> This is partially due to the oxygen sensitivity of many iron(II) complexes, which may preclude their handling under ambient laboratory conditions.

Given this paucity of literature on iron-mediated OMRP, it is not surprising that only a single report has described the polymerisation of either styrene or MMA under purely OMRP conditions (*i.e.* in the complete absence of halide).<sup>7d</sup> Table S3 presents the data obtained for the polymerisation of styrene under OMRP conditions using our range of iron(II) complexes and 1 equivalent of AIBN as the initiator. Most of the complexes tested exhibit little or no control over the OMRP of styrene, with the  $\bar{D}$  of these reactions being greater than 1.8. However, picolyl-containing complexes **3a** and **4a** display a moderate degree of control over the reactions, with  $\bar{D}$ s of 1.58 and 1.61 being achieved. This represents a much higher degree of control under these conditions than we were able to achieve using our best performing iron(II) amine-*bis*(phenolate) complex,<sup>7d</sup> and may suggest improved carbon radical trapping by these systems. The presence of a picolyl donor and HMDS ligand appear important, since switching either the tethered donor (to a tertiary amine or ether) or the ancillary donor (to an alkoxide/phenoxide) reduces control significantly. However, in all cases the theoretical molecular weights are somewhat lower than the values obtained *via* GPC, indicating loss of a significant number of radicals before an OMRP equilibrium is established.

Based on our previous findings,<sup>7d</sup> we anticipated that control over the OMRP of MMA would be much easier to achieve (than styrene) given the apparent greater affinity of iron complexes for MMA-type radicals. Table 1 illustrates the

screening data obtained for the OMRP of MMA under the same conditions as those used for styrene OMRP. It is evident that many of the complexes are reasonably efficient mediators

Table 1 MMA OMRP screening<sup>a</sup>



Entry	Complex	Conv. (%)	$M_{n,th}[AIBN]$ (Da)	$M_{n,th}[Fe]$ (Da)	$M_n$ (Da)	$\bar{D}$
1	<b>1a</b>	73	3654	7308	11764	1.47
2	<b>2a</b>	69	3454	6908	11704	1.37
3	<b>3a</b>	13	651	1302	13862	1.49
4	<b>4a</b>	22	1101	2202	11128	1.53
5	<b>1b</b>	56	2803	5606	10229	1.45
6	<b>3b</b>	36	1802	3604	10123	1.41
7	<b>1c</b>	54	2703	5406	10734	1.33
8	<b>3c</b>	9	451	902	<sup>b</sup>	<sup>b</sup>

<sup>a</sup> Conditions: [MMA]:[Fe]<sup>II</sup>:[AIBN] = 100:1.00:1.00, MMA:toluene = 1:1 (v/v), 110°C, 1 hour. Conversion determined by <sup>1</sup>H NMR spectroscopy.  $M_{n,th}[AIBN] = [MMA]_0 / (2 \times [AIBN]_0) \times M(MMA) \times \text{conversion}$ .  $M_{n,th}[Fe] = [MMA]_0 / [Fe] \times M(MMA) \times \text{conversion}$ . <sup>b</sup> Too little polymer obtained for GPC analysis.

of MMA OMRP, with  $\bar{D}$ s of <1.53 for all complexes tested. The picolyl-substituted complexes (**3a**, **4a**, **3b** and **3c**) lead to significantly lower conversions, however, than the amine and ether-tethered complexes. Complex **3c** specifically gave a very low conversion (9%) to polymer, with minimal solid visible after attempted precipitation in acidified methanol. The top performing complex was **1c** ( $\bar{D}$  = 1.33), where the electron-withdrawing terphenolate ligand can both sterically protect the iron centre and promote increased Lewis acidity and a stronger metal-carbon bond. Attempts were made to improve the performance of complex **1c** (entry 7, Tables 1 and 2). It was

Table 2 Optimisation of MMA OMRP using complex **1c**<sup>a</sup>

Entry	Initiator / Equiv.	Solvent	Conv. (%)	$M_{n,th}[AIBN]$ (Da)	$M_{n,th}[Fe]$ (Da)	$M_n$ (Da)	$\bar{D}$
7	AIBN / 1	toluene	54	2703	5406	10734	1.33
9	AIBN / 0.5	toluene	20	2002	2002	10376	1.23
10	V-601 / 1	toluene	62	3104	6208	12672	1.35
11 <sup>b</sup>	V-65 / 1	toluene	55	2753	5506	11112	1.34
12	AIBN / 1	THF	67	3354	6708	10545	1.57
13	AIBN / 1	<i>neat</i>	70	3504	7008	13628	5.13 <sup>c</sup>
14 <sup>d</sup>	AIBN / 1	toluene	68	3404	13616	11605	1.56
15	AIBN / 1	toluene <sup>e</sup>	43	2153	4306	9755	1.38

<sup>a</sup> Conditions: [MMA]:[Fe]<sup>II</sup>:[initiator] = 100:1.00:X, MMA:solvent = 1:1 (v/v), 110°C, 1 hour. Conversion determined by <sup>1</sup>H NMR spectroscopy.  $M_{n,th}[AIBN] = [MMA]_0 / (2 \times [AIBN]_0) \times M(MMA) \times \text{conversion}$ .  $M_{n,th}[Fe] = [MMA]_0 / [Fe] \times M(MMA) \times \text{conversion}$ . <sup>b</sup> Reaction performed for 2 hours at 90 °C. <sup>c</sup> Bimodal distribution. <sup>d</sup> 0.5 equivalents of **1c**. <sup>e</sup> MMA:toluene = 1:2 (v/v).

observed that halving the number of equivalents of AIBN (entry 9, Table 2) led to a decrease in  $\bar{D}$  (to 1.23) and, as expected, a decrease in conversion. Since each molecule of AIBN generates two radicals upon thermal decomposition, at a ratio of 1:1 (AIBN:Fe) there are two radicals per iron(II) centre. This excess of radicals (with respect to iron(II)) should result in more termination at the early stages of the reaction. However, by halving the amount of AIBN (entry 9, Table 2), there is no longer an excess of radicals per iron(II) centre, which may help reduce termination reactions and thus improve dispersity. The use of the alternative radical initiators, V-601 (10 hour  $t_{1/2}$  = 66°C), a non-nitrile initiator with a similar decomposition profile to AIBN or V-65 (10 hour  $t_{1/2}$  = 51°C), a lower temperature radical initiator, led to very similar results to those obtained with AIBN (entries 10 and 11, Table 2). Note that the reaction using V-65 was performed for 2 hours at a lower temperature (90°C), since we anticipated a lower rate of propagation and thus slower conversion to polymer. At this lower temperature, it appears that trapping of the propagating radicals is as efficient and reversible as at the higher reaction temperature. Given the rapid rate of initiator decomposition at these temperatures, this should leave the decomposition of the so-formed organometallic complex as the only source of radicals. Thus it is likely that the reaction proceeds *via* an RT-OMRP (reversible termination-OMRP) mechanism rather than a DT-OMRP mechanism (degenerative transfer-OMRP). The use of THF (entry 12) as solvent, or performing the reaction in the bulk (entry 13) both had deleterious on reaction control, raising  $\bar{D}$  to 1.57 and 5.13 respectively. These results together imply that minimal stabilisation of the metal centre occurs in the presence of coordinating solvent, and that in the absence of solvent (or in the presence of a relatively volatile solvent (THF)), propagation and bimolecular coupling of radical chains are rapid giving high conversions and broad  $\bar{D}$ . However, doubling the volume of additional solvent (entry 15) had no further positive effect on control over the reaction.

As described previously, complex **3c** gave an especially poor conversion to polymer, even with the use of an excess of radical initiator. We sought to examine the fate of complex **3c** and thus, presumably, the reason for this low conversion by reacting it with MMA-type radicals, which can be generated by thermal decomposition of the azo initiator, V-601. The reaction was observed to darken over time, and an amount of black solid along with a small number of black crystals could be obtained *via* vapour diffusion of *n*-hexane in to the crude reaction mixture (Figure 5). The molecular structure of the complex obtained (**3c'**) illustrates a monomeric iron(III) complex, bearing two terphenolate donors. Of particular note in this structure is the substitution of a picolyl H atom for a methyl isobutyrate group, the methyl isobutyrate being derived from the decomposition of V-601. While it is difficult to speculate on the origin of this complex without further experimental corroboration, we suggest that it is likely formed *via* initial H atom abstraction by one equivalent of methyl isobutyrate radical, followed by radical-radical combination of the so-formed  $\beta$ -ketiminate-derived radical with a further methyl isobutyrate radical. The addition of a further methyl

isobutyrate group to the picolyl tether is likely precluded by steric factors. The loss of radicals *via* reaction with the ligand

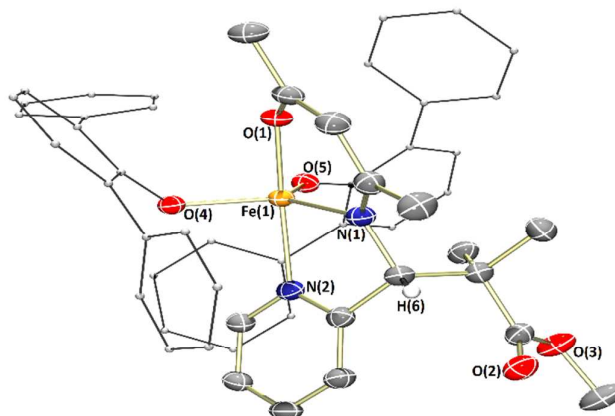


**Figure 5** Molecular structures of **3c'** with ellipsoids set at the 50% probability level. Hydrogen atoms (except picolyl H atom) have been omitted for clarity. Terphenolate rings represented in ball and stick form for clarity. Selected bond lengths (Å): **3c'** - Fe1-O1 1.9376(12), Fe1-O4 1.8995(12), Fe1-O5 1.8554(12), Fe1-N1 2.0856(15), Fe1-N2 2.1341(14).

scaffold in this manner will certainly suppress productive polymerisation, hence accounting for the very low conversion obtained for complex **3c**. This type of reactivity may account for the lower conversions obtained using the other complexes bearing picolyl tethers (cf. entries 3, 4, 6 and 8, Table 1).

While the lower dispersities in most OMRP reactions described here imply some level of control over the radical polymerisation, the deviation from unity also suggests that termination reactions must be occurring. This is further supported by kinetic analysis of the OMRP of MMA mediated by complex **1a** (see Supporting Information), which shows that molecular weights top out at higher conversions. Thus, catalytic chain transfer events are kinetically competitive with propagation, as has been observed previously in  $\alpha$ -diimine iron systems.<sup>25</sup>

## Conclusions

A series of donor-tethered tridentate  $\beta$ -ketiminate ligands have been synthesised and coordinated to iron(II) to afford four-coordinate complexes bearing a coordinated *bis*(trimethylsilyl)amide group. Protonolysis of these complexes with either benzyl alcohol or 2,6-diphenylphenol led to the formation of dimeric iron(II) complexes. All of the complexes synthesised were examined as mediators of styrene and methyl methacrylate polymerisation under both ATRP, and OMRP conditions. While all complexes were generally very poor mediators of ATRP,  $\bar{D}$ s as low as 1.23 could be achieved in the OMRP of MMA. Furthermore, through crystallographic characterisation of a decomposition product, we provide evidence that the presence of reactive picolyl H atoms may have a detrimental effect on a complex's ability to act as an efficient mediator of CRP. Clear design principles to manage

metal-halogen and metal-carbon bond strengths are emerging and continue to guide our design of iron-based catalysts in promoting controlled radical polymerisation and limiting chain transfer. As we understand the role of these complexes in controlling radical chemistry, we can consider applying them to other transformations. In particular, the application of these complexes (**1a** – **3c**) as catalysts for small molecule transformations invoking radical chemistry is also an area of interest to our group,<sup>26</sup> and will underpin future studies.

## Experimental

### Materials and methods

All experiments involving moisture- and air-sensitive compounds were performed under a nitrogen atmosphere using an MBraun LABmaster sp glovebox system equipped with a -35 °C freezer and [H<sub>2</sub>O] and [O<sub>2</sub>] analysers or using standard Schlenk techniques. Solvents used were obtained from a solvent purification system (Innovative Technologies) consisting of columns of alumina and copper catalyst and were further degassed by three freeze–pump–thaw cycles prior to use. Benzene-*d*<sub>6</sub> and THF-*d*<sub>8</sub> were dried by stirring over sodium/benzophenone, before being collected by distillation and degassed by three freeze–pump–thaw cycles. Chloroform-*d*<sub>1</sub> was used as received. Styrene and methyl methacrylate (MMA) were dried by stirring over calcium hydride for a minimum of 24 hours, before being vacuum transferred and stored at -35 °C. 2,2'-Azobis(2-methylpropionitrile) (AIBN), V-601 (Wako) and V-65 (Wako) were recrystallised from DCM/hexane, dried under vacuum and stored at -35 °C. (1-Chloroethyl)benzene (1-PECl) and benzyl alcohol were dried by stirring over calcium hydride for a minimum of 24 hours, before being distilled. [Fe(N(SiMe<sub>3</sub>)<sub>2</sub>)<sub>2</sub>THF] was synthesised using a modified literature procedure.<sup>18</sup> (4-Methoxy-pyridin-2-yl)methanamine was synthesised using a literature procedure.<sup>27</sup> Following purification, all reagents described above were stored under an inert atmosphere. 2,6-Diphenylphenol, acetylacetone, *N,N*-dimethylethylenediamine, 2-picolyamine and tetrahydrofurfurylamine were all used as received. Gel permeation chromatography (GPC) was carried out in THF at a flow rate of 1 mL min<sup>-1</sup> at 35 °C on a Malvern Instruments Viscotek 270 GPC Max triple detection system with 2 × mixed bed styrene/DVB columns (300 × 7.5 mm). Absolute molar masses were obtained using dn/dc values of 0.185 for poly(styrene)<sup>28</sup> and 0.088 for poly(methyl methacrylate).<sup>29</sup> NMR spectra were obtained on either a 400 MHz or 500 MHz Bruker Avance III spectrometer. Solution magnetic moments were determined *via* NMR spectroscopy using Evans' method.<sup>30</sup> Mass spectra were obtained on a Bruker Daltonics micro TOF instrument operating in the positive ion electrospray mode. Elemental analyses were performed by Stephen Boyer at London Metropolitan University.

### Synthetic procedures

#### General protocol for synthesis of ligand precursors L1H–L4H.

Equimolar amounts of acetylacetone and amine were dissolved in methanol, with the resulting solution being heated at reflux with stirring for 24 hours. After this time, the yellow solution obtained was cooled to ambient temperature and the volatiles removed *in vacuo*. The resulting yellow oil was taken up in dichloromethane and the solution dried over MgSO<sub>4</sub>. The MgSO<sub>4</sub> was then removed by filtration and the dichloromethane was removed *in vacuo* to give the crude product as a yellow oil. **L1H** and **L2H** were further purified and obtained as pale yellow oils by distillation under high vacuum. **L3H** and **L4H** were further purified and obtained as colourless crystalline solids by storage at -30 °C in a minimum of an equimolar solution of diethyl ether/*n*-hexane.

**Data for L4H:** <sup>1</sup>H NMR (500 MHz, CDCl<sub>3</sub>) δ 11.21 (br s, 1H, NH), 8.36 (d, *J* = 5.7 Hz, 1H, pyH), 6.77 (d, *J* = 2.4 Hz, 1H, pyH), 6.69 (dd, *J* = 5.7, 2.4 Hz, 1H, pyH), 5.06 (s, 1H), 4.52 (d, *J* = 6.5 Hz, 2H, NCH<sub>2</sub>Py), 3.82 (s, 3H, OCH<sub>3</sub>), 2.03 (s, 3H, CCH<sub>3</sub>), 1.92 (s, 3H, CCH<sub>3</sub>) ppm. <sup>13</sup>C{<sup>1</sup>H} NMR (126 MHz, CDCl<sub>3</sub>) δ 195.8, 166.8, 163.1, 159.8, 150.9, 108.5, 107.0, 96.4, 55.3, 48.7, 29.1, 19.1 ppm. HRMS (ESI<sup>+</sup>): *m/z* 221.1296 [M + H]<sup>+</sup> calculated [M + H]<sup>+</sup> 221.1285. Characterisation data for **L1H**,<sup>10a</sup> **L2H**<sup>10b</sup> and **L3H**<sup>31</sup> was found to be in agreement with that reported in the literature.

**Synthesis of [Fe(L1)(N(SiMe<sub>3</sub>)<sub>2</sub>)] (1a).** To a solution of [Fe(N(SiMe<sub>3</sub>)<sub>2</sub>)<sub>2</sub>THF] (200 mg, 0.45 mmol) in *n*-hexane (2 ml) was added a solution of **L1H** (75.9 mg, 0.45 mmol) in *n*-hexane (2 ml) with stirring. The resultant solution was stirred at room temperature for 30 minutes. After this time, the solution was placed in a freezer at -35 °C, inducing the crystallisation of the product as large, green blocks, which were collected and dried *in vacuo* (144 mg, 0.37 mmol, 84%). A single crystal suitable for X-ray diffraction analysis was selected from the bulk material. <sup>1</sup>H NMR (500 MHz, C<sub>6</sub>D<sub>6</sub>) δ 160.30, 96.46, 85.63, 6.32, -19.48, -28.34, -57.41 ppm.  $\mu_{eff}$  (Evans' Method, C<sub>6</sub>D<sub>6</sub>) = 4.9  $\mu_B$ . Analysis Calculated for C<sub>15</sub>H<sub>35</sub>FeN<sub>3</sub>OSi<sub>2</sub>: C, 46.74; H, 9.15; N, 10.90. Found: C, 46.61; H, 9.20; N, 10.82.

**Synthesis of [Fe(L2)(N(SiMe<sub>3</sub>)<sub>2</sub>)] (2a).** To a solution of [Fe(N(SiMe<sub>3</sub>)<sub>2</sub>)<sub>2</sub>THF] (400 mg, 0.89 mmol) in *n*-hexane (4 ml) was added a solution of **L2H** (163 mg, 0.89 mmol) in *n*-hexane (4 ml) with stirring. The resultant solution was stirred at room temperature for 30 minutes. After this time, the volatiles were removed *in vacuo*, yielding a green crystalline solid (341 mg, 0.86 mmol, 96%). Single crystals suitable for X-ray diffraction analysis were obtained on cooling a saturated *n*-hexane solution of the product to -35 °C. <sup>1</sup>H NMR (500 MHz, C<sub>6</sub>D<sub>6</sub>) δ 69.51, 30.03, 21.59, 19.92, 16.09, 14.97, 12.20, 10.61, 4.44, 3.92, 2.79, -3.90, -15.29, -23.47 ppm.  $\mu_{eff}$  (Evans' Method, C<sub>6</sub>D<sub>6</sub>) = 5.3  $\mu_B$ . Analysis Calculated for C<sub>16</sub>H<sub>34</sub>FeN<sub>2</sub>O<sub>2</sub>Si<sub>2</sub>: C, 48.23; H, 8.60; N, 7.03. Found: C, 48.17; H, 8.68; N, 6.91.

**Synthesis of [Fe(L3)(N(SiMe<sub>3</sub>)<sub>2</sub>)] (3a).** To a solution of [Fe(N(SiMe<sub>3</sub>)<sub>2</sub>)<sub>2</sub>THF] (400 mg, 0.89 mmol) in *n*-hexane (3 ml) was added a solution of **L3H** (170 mg, 0.89 mmol) in *n*-hexane (17 ml) with stirring. The resultant mixture was stirred vigorously at room temperature for 1 hour. After this time, the solution was placed in a freezer at -35 °C to complete crystallisation of the product, which was obtained as green

needles following filtration and drying *in vacuo* (300 mg, 0.74 mmol, 83%). Single crystals suitable for X-ray diffraction analysis were obtained on cooling a saturated *n*-hexane solution of the product to  $-35^{\circ}\text{C}$ .  $^1\text{H NMR}$  (500 MHz,  $\text{THF-d}_8$ )  $\delta$  166.17, 89.42, 58.34, 56.52, 9.22, -6.61, -9.85, -13.48, -37.25 ppm.  $\mu_{\text{eff}}$  (Evans' Method,  $\text{C}_6\text{D}_6$ ) = 5.0  $\mu_{\text{B}}$ . Analysis Calculated for  $\text{C}_{17}\text{H}_{31}\text{FeN}_3\text{OSi}_2$ : C, 50.36; H, 7.71; N, 10.36. Found: C, 50.12; H, 7.52; N, 10.17.

**Synthesis of [Fe(L4)(N(SiMe<sub>3</sub>)<sub>2</sub>)] (4a).** To a solution of [Fe(N(SiMe<sub>3</sub>)<sub>2</sub>)<sub>2</sub>THF] (200 mg, 0.45 mmol) in toluene (5 ml) was added a solution of L4H (98.2 mg, 0.45 mmol) in toluene (5 ml) with stirring. The resultant solution was stirred at room temperature for 1 hour. After this time, the volatiles were removed *in vacuo*, yielding the crude product as a green oily solid. Dissolution of this in a minimum of *n*-hexane, followed by storage at  $-35^{\circ}\text{C}$  overnight gave the pure product as green crystals (141 mg, 0.32 mmol, 72%). A single crystal suitable for X-ray diffraction analysis was selected from the bulk material.  $^1\text{H NMR}$  (500 MHz,  $\text{C}_6\text{D}_6$ )  $\delta$  167.48, 82.93, 55.49, 50.91, 8.47, 3.70, -5.61, -13.46, -39.60 ppm.  $\mu_{\text{eff}}$  (Evans' Method,  $\text{C}_6\text{D}_6$ ) = 5.4  $\mu_{\text{B}}$ . Analysis Calculated for  $\text{C}_{18}\text{H}_{33}\text{FeN}_3\text{O}_2\text{Si}_2$ : C, 49.64; H, 7.64; N, 9.65. Found: C, 49.43; H, 7.43; N, 9.46.

**Synthesis of [Fe(L1)OBn] (1b).** Complex 1a (101 mg, 0.26 mmol) was taken-up in *n*-hexane (4 ml). To this was added an *n*-hexane (2 ml) solution of benzyl alcohol (32.4 mg, 0.30 mmol) with stirring. The resultant mixture was stirred at room temperature for 30 minutes, during which time an orange crystalline solid formed. After this time, the reaction mixture was placed in a freezer at  $-35^{\circ}\text{C}$  for 18 hours to complete crystallisation of the product. The resulting orange crystalline solid was collected and dried *in vacuo* (74.5 mg, 0.22 mmol, 86%). Single crystals suitable for X-ray diffraction analysis were obtained on cooling of a saturated solution of the compound in *n*-hexane at reflux.  $^1\text{H NMR}$  (500 MHz,  $\text{C}_6\text{D}_6$ )  $\delta$  136.96, 119.92, 106.46, 67.36, 41.35, 16.22, 8.76, 3.31, 0.49, -1.45, -2.59, -3.07, -4.15, -5.10, -5.53, -13.29, -23.32, -27.94, -30.86, -33.45, -42.26 ppm.  $\mu_{\text{eff}}$  (Evans' Method,  $\text{C}_6\text{D}_6$ ) = 5.4  $\mu_{\text{B}}$ . Analysis Calculated for  $\text{C}_{16}\text{H}_{24}\text{FeN}_2\text{O}_2$ : C, 57.85; H, 7.28; N, 8.43. Found: C, 58.02; H, 7.13; N, 8.59.

**Synthesis of [Fe(L3)OBn] (3b).** Complex 3a (100 mg, 0.25 mmol) was taken-up in *n*-hexane (5 ml). To this was added an *n*-hexane (2 ml) solution of benzyl alcohol (26.7 mg, 0.25 mmol) with stirring. On addition of benzyl alcohol, the reaction mixture immediately changed colour (to red), and a large amount of red precipitate formed. The resultant suspension was stirred vigorously at room temperature for 1 hour. The red solid was collected by filtration and was dried *in vacuo* (83.1 mg, 0.24 mmol, 96%).  $\mu_{\text{eff}}$  (Evans' Method,  $\text{THF-d}_8$ ) = 5.2  $\mu_{\text{B}}$ . Analysis Calculated for  $\text{C}_{18}\text{H}_{20}\text{FeN}_2\text{O}_2$ : C, 61.38; H, 5.72; N, 7.95. Found: C, 61.29; H, 5.61; N, 7.88.<sup>32</sup>

**Synthesis of [Fe(L1)OTer] (1c).** Complex 1a (112 mg, 0.29 mmol) was taken-up in toluene (2 ml). To this was added a toluene (2 ml) solution of 2,6-diphenylphenol (71.6 mg, 0.29 mmol) with stirring. The resultant mixture was stirred at room temperature for 1 hour. After this time the volatiles were removed *in vacuo*. The resultant residue was recrystallised from toluene/*n*-hexane, giving the pure product as a yellow-

orange, microcrystalline powder (99.1 mg, 0.21 mmol, 73%). Single crystals suitable for X-ray diffraction analysis were obtained on storage of a concentrated solution of the compound in toluene/*n*-hexane at  $-35^{\circ}\text{C}$ .  $^1\text{H NMR}$  (500 MHz,  $\text{THF-d}_8$ )  $\delta$  71.77, 68.69, 36.83, 21.33, 6.51, 3.74, -1.15, -8.51, -17.29, -22.44, -30.07 ppm.  $\mu_{\text{eff}}$  (Evans' Method,  $\text{C}_6\text{D}_6$ ) = 5.1  $\mu_{\text{B}}$ . Analysis Calculated for  $\text{C}_{27}\text{H}_{30}\text{FeN}_2\text{O}_2$ : C, 68.94; H, 6.43; N, 5.96. Found: C, 69.06; H, 6.56; N, 6.01.

**Synthesis of [Fe(L3)OTer] (3c).** A solution of complex 3a (80.0 mg, 0.20 mmol) and 2,6-diphenylphenol (48.6 mg, 0.20 mmol) in toluene (2 ml) was stirred at room temperature for 2 hours, during which time, a small amount of orange crystalline powder had formed. After this time, *n*-hexane (15 ml) was added with stirring, and the resultant orange microcrystalline solid was collected by filtration, washed with *n*-hexane (3 ml) and dried *in vacuo* (70.8 mg, 0.14 mmol, 73%). Single crystals suitable for X-ray diffraction analysis were obtained on storage of a concentrated solution of the compound in toluene/*n*-hexane at  $-35^{\circ}\text{C}$ .  $^1\text{H NMR}$  (500 MHz,  $\text{THF-d}_8$ )  $\delta$  52.17, 51.31, 35.42, 29.53, 24.05, 21.63, 5.96, -1.91, -12.22, -21.80, -41.07.  $\mu_{\text{eff}}$  (Evans' Method,  $\text{C}_6\text{D}_6$ ) = 4.8  $\mu_{\text{B}}$ .<sup>33</sup> Analysis Calculated for  $\text{C}_{29}\text{H}_{26}\text{FeN}_2\text{O}_2$ : C, 71.03; H, 5.34; N, 5.71. Found: C, 71.16; H, 5.40; N, 5.68.

**Synthesis of 3c'.** A solution of complex 3c (21.3 mg) and V-601 (30.0 mg) in toluene (1 ml) was heated with stirring at  $90^{\circ}\text{C}$  for 2 hours. After this time, the mixture was cooled and *n*-hexane was allowed to diffuse in to the crude reaction mixture at ambient temperature, producing a black solid and a number of black crystals.

#### CRP Procedures

##### General procedure for ATRP of styrene or MMA

In a glovebox, a small ampoule was charged with iron(II) complex (24.0  $\mu\text{mol}$ ), monomer (2.40 mmol) and toluene (toluene:monomer, 1:1, v/v). To this was added 1-PECL (24.0  $\mu\text{mol}$ ) by microsyringe. The ampoule was brought out of the glovebox and heated at  $120^{\circ}\text{C}$  for 1 hour with a stir-rate of 500 rpm. After this time, the ampoule was cooled rapidly to ambient temperature, and an aliquot removed for analysis by  $^1\text{H NMR}$  spectroscopy to determine monomer conversion. The remainder of the reaction mixture was dissolved in a small volume of THF (ca. 2 ml), and the polymer precipitated by addition of the THF solution to acidified methanol ( $\text{MeOH:HCl}_{(\text{aq})}$ , ca. 75 ml:1 ml). The polymer was collected by filtration and dried *in vacuo*.

##### General procedure for OMRP of styrene or MMA

In a glovebox, a small ampoule was charged with iron(II) complex (24.0  $\mu\text{mol}$ ), monomer (2.40 mmol), toluene (toluene:monomer, 1:1, v/v) and AIBN (24.0  $\mu\text{mol}$ ). The ampoule was brought out of the glovebox and heated at  $110^{\circ}\text{C}$  for 1 hour with a stir-rate of 500 rpm. After this time, the ampoule was cooled rapidly to ambient temperature, and an aliquot removed for analysis by  $^1\text{H NMR}$  spectroscopy to determine monomer conversion. The remainder of the reaction mixture was taken-up in a small volume of THF (ca. 2 ml), and the polymer precipitated by addition of the THF

solution to acidified methanol (MeOH:HCl<sub>(aq)</sub>, ca. 75 ml:1 ml). The polymer was collected by filtration and dried *in vacuo*.

### Crystallography

X-Ray diffraction data was collected on an Agilent SuperNova diffractometer fitted with an Atlas CCD detector with Mo-K<sub>α</sub> radiation ( $\lambda = 0.7107 \text{ \AA}$ ) or Cu-K<sub>α</sub> radiation ( $\lambda = 1.5418 \text{ \AA}$ ). Crystals were mounted under paratone on MiTeGen loops. The structures were solved by direct methods using SHELXS or SHELXT interfaced through Olex2 and refined by full-matrix least-squares on F2 using SHELXL, interfaced through Olex2.<sup>34</sup> Molecular graphics for all structures were generated using POV-RAY, POVLabel and Ortep.

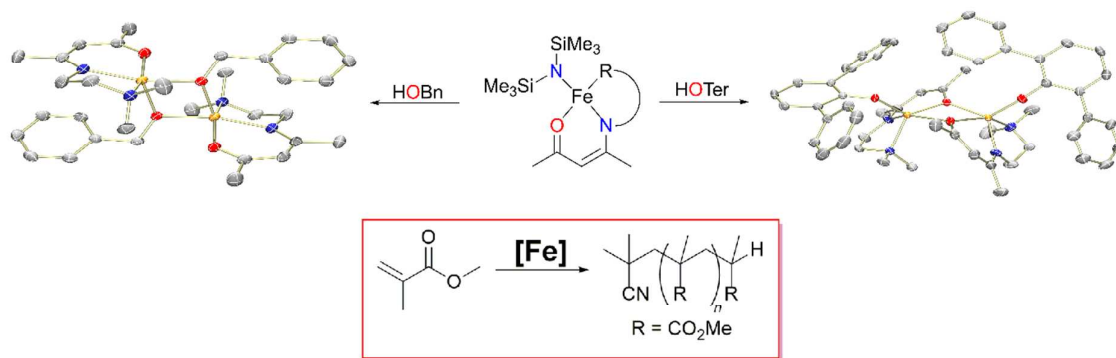
### Acknowledgements

M.P.S. and B.R.M.L. gratefully acknowledge support from the EPSRC (EP/M000842/1), a Marie Curie Career Integration Grant (FP7-PEOPLE-2013-CIG-618372) and the University of Edinburgh for financial support. We thank Dr Gary Nichol for collection of the X-ray diffraction data. We also thank Wako Chemicals GmbH for providing us with samples of the initiators V-601 and V-65, and Synthomer for useful discussions.

### Notes and references

- (a) I. Bauer and H.-J. Knölker, *Chemical Reviews*, 2015, **115**, 3170-3387; (b) I. Bauer and H.-J. Knölker, in *Iron Catalysis in Organic Chemistry*, Wiley-VCH Verlag GmbH & Co. KGaA, 2008, pp. 1-27; (c) C. Bolm, J. Legros, J. Le Pailh and L. Zani, *Chemical Reviews*, 2004, **104**, 6217-6254; (d) J. Gui, C.-M. Pan, Y. Jin, T. Qin, J. C. Lo, B. J. Lee, S. H. Spengel, M. E. Mertzman, W. J. Pitts, T. E. La Cruz, M. A. Schmidt, N. Darvatkar, S. R. Natarajan and P. S. Baran, *Science*, 2015, **348**, 886-891; (e) J. M. Hoyt, V. A. Schmidt, A. M. Tondreau and P. J. Chirik, *Science*, 2015, **349**, 960-963; (f) R. Pony Yu, D. Hesk, N. Rivera, I. Pelczer and P. J. Chirik, *Nature*, 2016, **529**, 195-199; (g) X. Jia and Z. Huang, *Nat Chem*, 2016, **8**, 157-161; (h) A. Sharma and J. F. Hartwig, *Nature*, 2015, **517**, 600-604.
- (a) J.-S. Wang and K. Matyjaszewski, *Journal of the American Chemical Society*, 1995, **117**, 5614-5615; (b) J.-S. Wang and K. Matyjaszewski, *Macromolecules*, 1995, **28**, 7901-7910.
- (a) M. Kato, M. Kamigaito, M. Sawamoto and T. Higashimura, *Macromolecules*, 1995, **28**, 1721-1723; (b) T. Ando, M. Kato, M. Kamigaito and M. Sawamoto, *Macromolecules*, 1996, **29**, 1070-1072.
- (a) T. Ando, M. Kamigaito and M. Sawamoto, *Macromolecules*, 1997, **30**, 4507-4510; (b) K. Matyjaszewski, M. Wei, J. Xia and N. E. McDermott, *Macromolecules*, 1997, **30**, 8161-8164; (c) Y. Kotani, M. Kamigaito and M. Sawamoto, *Macromolecules*, 1999, **32**, 6877-6880; (d) B. Göbel and K. Matyjaszewski, *Macromolecular Chemistry and Physics*, 2000, **201**, 1619-1624; (e) J. Louie and R. H. Grubbs, *Chemical Communications*, 2000, 1479-1480; (f) M. Teodorescu, S. G. Gaynor and K. Matyjaszewski, *Macromolecules*, 2000, **33**, 2335-2339; (g) G. Moineau, P. Dubois, R. Jérôme, T. Senninger and P. Teyssié, *Macromolecules*, 1998, **31**, 545-547; (h) J. Xia, H.-j. Paik and K. Matyjaszewski, *Macromolecules*, 1999, **32**, 8310-8314.
- (a) Z. Xue, D. He and X. Xie, *Polymer Chemistry*, 2015, **6**, 1660-1687; (b) B. R. M. Lake and M. P. Shaver, in *Controlled Radical Polymerization: Mechanisms*, American Chemical Society, 2015, vol. 1187, ch. 17, pp. 311-326; (c) R. Poli, L. E. N. Allan and M. P. Shaver, *Progress in Polymer Science*, 2014, **39**, 1827-1845.
- (a) L. E. N. Allan, J. P. MacDonald, A. M. Reckling, C. M. Kozak and M. P. Shaver, *Macromolecular Rapid Communications*, 2012, **33**, 414-418; (b) L. E. N. Allan, J. P. MacDonald, G. S. Nichol and M. P. Shaver, *Macromolecules*, 2014, **47**, 1249-1257.
- (a) R. Poli and M. P. Shaver, *Inorganic Chemistry*, 2014, **53**, 7580-7590; (b) H. Schroeder and M. Buback, *Macromolecules*, 2015, **48**, 6108-6113; (c) H. Schroeder, M. Buback and M. P. Shaver, *Macromolecules*, 2015, **48**, 6114-6120; (d) H. Schroeder, B. R. M. Lake, S. Demeshko, M. P. Shaver and M. Buback, *Macromolecules*, 2015, **48**, 4329-4338.
- J.-I. Lee, T.-Y. Lee, L.-C. Chang, C.-Y. Lin, H. M. Lee, L. Hung, A. Datta and J.-H. Huang, *Journal of Molecular Structure*, 2009, **929**, 207-212.
- R. Poli, *Chemistry – A European Journal*, 2015, **21**, 6988-7001.
- (a) S. Gulli, J.-C. Daran and R. Poli, *European Journal of Inorganic Chemistry*, 2011, **2011**, 1666-1672; (b) H.-C. Tseng, M. Y. Chiang, W.-Y. Lu, Y.-J. Chen, C.-J. Lian, Y.-H. Chen, H.-Y. Tsai, Y.-C. Lai and H.-Y. Chen, *Dalton Transactions*, 2015, **44**, 11763-11773; (c) Y. Yamaguchi, H. Ando, M. Nagaya, H. Hinago, T. Ito and M. Asami, *Chemistry Letters*, 2011, **40**, 983-985.
- D. M. Granum, P. J. Riedel, J. A. Crawford, T. K. Mahle, C. M. Wyss, A. K. Begej, N. Arulsamy, B. S. Pierce and M. P. Mehn, *Dalton Transactions*, 2011, **40**, 5881-5890.
- (a) S. J. J. Titinchi, G. Von Willingh, H. S. Abbo and R. Prasad, *Catalysis Science & Technology*, 2015, **5**, 325-338; (b) A. Ray, G. Pilet, C. J. Gómez-García and S. Mitra, *Polyhedron*, 2009, **28**, 511-520.
- C. Scheiper, D. Dittich, C. Wölper, D. Bläser, J. Roll and S. Schulz, *European Journal of Inorganic Chemistry*, 2014, **2014**, 2230-2240.
- T. Akashi, J. Nakazawa and S. Hikichi, *Journal of Molecular Catalysis A: Chemical*, 2013, **371**, 42-47.
- L. Yang, D. R. Powell and R. P. Houser, *Dalton Transactions*, 2007, 955-964.
- (a) J. Cirera, P. Alemany and S. Alvarez, *Chemistry – A European Journal*, 2004, **10**, 190-207; (b) J. Cirera, E. Ruiz and S. Alvarez, *Inorganic Chemistry*, 2008, **47**, 2871-2889.
- A. F. Lugo and A. F. Richards, *Inorganica Chimica Acta*, 2010, **363**, 2104-2112.
- M. M. Olmstead, P. P. Power and S. C. Shoner, *Inorganic Chemistry*, 1991, **30**, 2547-2551.
- (a) S. A. Sulway, D. Collison, J. J. W. McDouall, F. Tuna and R. A. Layfield, *Inorganic Chemistry*, 2011, **50**, 2521-2526; (b) G. Jin, L. Vendier, Y. Coppel, S. Sabo-Etienne and S. Bontemps, *Dalton Transactions*, 2015, **44**, 7500-7505; (c) B. A. Frazier, P. T. Wolczanski, E. B. Lobkovsky and T. R. Cundari, *Journal of the American Chemical Society*, 2009, **131**, 3428-3429; (d) B. A. Frazier, V. A. Williams, P. T.

- Wolczanski, S. C. Bart, K. Meyer, T. R. Cundari and E. B. Lobkovsky, *Inorganic Chemistry*, 2013, **52**, 3295-3312.
- 20 (a) D. J. Darensbourg, C. G. Ortiz and D. R. Billodeaux, *Inorganica Chimica Acta*, 2004, **357**, 2143-2149; (b) P. Zhao, H. Lei, C. Ni, J.-D. Guo, S. Kamali, J. C. Fettinger, F. Grandjean, G. J. Long, S. Nagase and P. P. Power, *Inorganic Chemistry*, 2015, **54**, 8914-8922; (c) J. S. Figueroa, J. G. Melnick and G. Parkin, *Inorganic Chemistry*, 2006, **45**, 7056-7058; (d) T. J. Boyle, L. A. M. Ottley, C. A. Apblett, C. A. Stewart, S. M. Hoppe, K. L. Hawthorne and M. A. Rodriguez, *Inorganic Chemistry*, 2011, **50**, 6174-6182; (e) C. Ni and P. P. Power, *Chemical Communications*, 2009, 5543-5545.
- 21 (a) E. M. Townsend, R. R. Schrock and A. H. Hoveyda, *Journal of the American Chemical Society*, 2012, **134**, 11334-11337; (b) R. R. Schrock, A. J. Jiang, S. C. Marinescu, J. H. Simpson and P. Müller, *Organometallics*, 2010, **29**, 5241-5251; (c) J. McKinven, G. S. Nichol and P. L. Arnold, *Dalton Transactions*, 2014, **43**, 17416-17421.
- 22 (a) F. di Lena and K. Matyjaszewski, *Progress in Polymer Science*, 2010, **35**, 959-1021; (b) R. Poli, *European Journal of Inorganic Chemistry*, 2011, **2011**, 1513-1530.
- 23 (a) L. E. N. Allan, M. R. Perry and M. P. Shaver, *Progress in Polymer Science*, 2012, **37**, 127-156; (b) R. Poli and M. P. Shaver, *Chemistry – A European Journal*, 2014, **20**, 17530-17540.
- 24 (a) J. Wang, J. Zhou, H. S. E. M. Sharif, D. He, Y. S. Ye, Z. Xue and X. Xie, *RSC Advances*, 2015, **5**, 96345-96352; (b) Z. Xue and R. Poli, *Journal of Polymer Science Part A: Polymer Chemistry*, 2013, **51**, 3494-3504.
- 25 (a) M. P. Shaver, L. E. N. Allan, H. S. Rzepa and V. C. Gibson, *Angewandte Chemie International Edition*, 2006, **45**, 1241-1244; (b) L. E. N. Allan, M. P. Shaver, A. J. P. White and V. C. Gibson, *Inorganic Chemistry*, 2007, **46**, 8963-8970; (c) R. Poli and M. P. Shaver, *Chemistry – A European Journal*, 2014, **20**, 17530-17540.
- 26 (a) K. Zhu, M. P. Shaver and S. P. Thomas, *European Journal of Organic Chemistry*, 2015, **10**, 2119-2123; (b) K. Zhu, M. P. Shaver and S. P. Thomas, *Chemistry – An Asian Journal*, 2016, **11**, 977-980; (c) K. Zhu, M. P. Shaver and S. P. Thomas, *Chemical Science*, 2016, DOI: 10.1039/C5SC04471E.
- 27 C. X. Zhang, S. Kaderli, M. Costas, E.-i. Kim, Y.-M. Neuhold, K. D. Karlin and A. D. Zuberbühler, *Inorganic Chemistry*, 2003, **42**, 1807-1824.
- 28 S. Grcev, P. Schoenmakers and P. Iedema, *Polymer*, 2004, **45**, 39-48.
- 29 K. Min, H. Gao, J. A. Yoon, W. Wu, T. Kowalewski and K. Matyjaszewski, *Macromolecules*, 2009, **42**, 1597-1603.
- 30 D. F. Evans, *Journal of the Chemical Society (Resumed)*, 1959, 2003-2005.
- 31 V. A. Williams, P. T. Wolczanski, J. Sutter, K. Meyer, E. B. Lobkovsky and T. R. Cundari, *Inorganic Chemistry*, 2014, **53**, 4459-4474.
- 32 Due to relatively poor solubility in deuterated solvents (THF- $d_8$ ,  $C_6D_6$ ,  $CD_3CN$ ), we were unable to obtain a clear  $^1H$  NMR spectrum with an acceptable signal-to-noise ratio. We believe the low quality of the spectra obtained also results from solution fluxionality.
- 33 The solution magnetic moment ( $4.8 \mu_B$ ) determined for complex **3c** is slightly lower than might be expected for a  $d^6$  high-spin complex. We suggest this is caused by lattice solvent, which is not accounted for in the solution magnetic moment calculation. Using the information obtained from the SQUEEZE routine in the crystallographic software, PLATON, it is calculated that there is electron density pertaining to approximately 2.5 molecules of solvent toluene (or hexane) per unit cell, which equates to approximately 0.6 molecules of toluene per dimer. If 0.6 molecules of toluene are included in the solution magnetic moment calculation, a value of  $5.0 \mu_B$  is obtained.
- 34 (a) O. V. Dolomanov, L. J. Bourhis, R. J. Gildea, J. A. K. Howard and H. Puschmann, *Journal of Applied Crystallography*, 2009, **42**, 339-341; (b) G. Sheldrick, *Acta Crystallographica Section A*, 2015, **71**, 3-8; (c) G. Sheldrick, *Acta Crystallographica Section A*, 2008, **64**, 112-122.



A series of novel iron(II)- $\beta$ -ketiminate complexes have been prepared and shown to be efficient mediators of MMA CRP.

## Supporting Information

**Iron(II)- $\beta$ -ketiminate complexes as mediators of controlled radical polymerisation**Benjamin R. M. Lake<sup>a</sup> and Michael. P. Shaver\*<sup>a</sup><sup>a</sup>EaStCHEM School of Chemistry, University of Edinburgh, Edinburgh, EH9 EJJ, UK.**CONTENT****GPC DATA**

<b>Table S1</b>	ATRP of styrene
<b>Table S2</b>	ATRP of MMA
<b>Table S3</b>	OMRP of styrene
<b>Table S4</b>	OMRP of MMA

**KINETIC DATA**

<b>Figure S5</b>	First-order kinetic plot for the OMRP of MMA mediated by complex <b>1a</b>
------------------	--

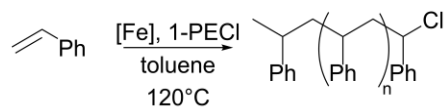
**NMR SPECTRA**

<b>Figure S6</b>	<sup>1</sup> H NMR spectrum of complex <b>1a</b> (500 MHz, C <sub>6</sub> D <sub>6</sub> )
<b>Figure S7</b>	<sup>1</sup> H NMR spectrum of complex <b>2a</b> (500 MHz, C <sub>6</sub> D <sub>6</sub> )
<b>Figure S8</b>	<sup>1</sup> H NMR spectrum of complex <b>3a</b> (500 MHz, THF-d <sub>8</sub> )
<b>Figure S9</b>	<sup>1</sup> H NMR spectrum of complex <b>4a</b> (500 MHz, C <sub>6</sub> D <sub>6</sub> )
<b>Figure S10</b>	<sup>1</sup> H NMR spectrum of complex <b>1b</b> (500 MHz, THF-d <sub>8</sub> )
<b>Figure S11</b>	<sup>1</sup> H NMR spectrum of complex <b>1c</b> (500 MHz, THF-d <sub>8</sub> )
<b>Figure S12</b>	<sup>1</sup> H NMR spectrum of complex <b>3c</b> (500 MHz, THF-d <sub>8</sub> )

**X-RAY CRYSTALLOGRAPHIC DATA**

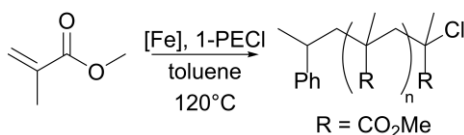
<b>Figure S13</b>	Complex <b>1a</b>
<b>Figure S14</b>	Complex <b>2a</b>
<b>Figure S15</b>	Complex <b>3a</b>
<b>Figure S16</b>	Complex <b>4a</b>
<b>Figure S17</b>	Complex <b>1b</b>
<b>Figure S18</b>	Complex <b>3b</b>
<b>Figure S19</b>	Complex <b>1c</b>
<b>Figure S20</b>	Complex <b>3c</b>
<b>Figure S21</b>	Complex <b>3c'</b>

## GPC DATA

Table S1 ATRP of styrene<sup>a</sup>

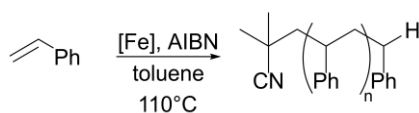
Entry	Complex	Conv. (%)	$M_{n,th}$ (Da)	$M_n$ (Da)	$\bar{D}$
S1	1a	34	3541	8362	1.78
S2	2a	24	2500	9377	1.76
S3	3a	22	2291	5366	1.66
S4	4a	23	2395	5892	1.74
S5	1b	23	2395	5057	1.69
S6	3b	19	1979	4935	1.70
S7	1c	21	2187	9312	1.74
S8	3c	24	2500	4661	1.81

<sup>a</sup> Conditions: [styrene]:[Fe<sup>II</sup>]:[1-PECl] = 100:1.00:1.00, styrene:toluene = 1:1 (v/v), 120°C, 1 hour. Conversion determined by <sup>1</sup>H NMR spectroscopy.  $M_{n,th}$  = [styrene]<sub>0</sub>/[1-PECl]<sub>0</sub> × M(styrene) × conversion.

Table S2 ATRP of MMA<sup>a</sup>

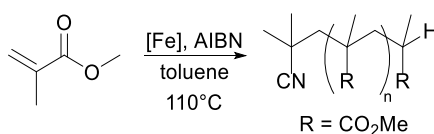
Entry	Complex	Conv. (%)	$M_{n,th}$ (Da)	$M_n$ (Da)	$\bar{D}$
S9	1a	70	7008	14792	1.81
S10	2a	57	5707	19283	2.18
S11	3a	40	4005	12368	1.45
S12	4a	43	4305	13386	1.61
S13	1b	54	5406	15021	1.60
S14	3b	35	3504	15184	1.41
S15	1c	37	3704	28168	2.22
S16	3c	41	4105	15288	1.78

<sup>a</sup> Conditions: [MMA]:[Fe<sup>II</sup>]:[1-PECl] = 100:1.00:1.00, MMA:toluene = 1:1 (v/v), 120°C, 1 hour. Conversion determined by <sup>1</sup>H NMR spectroscopy.  $M_{n,th}$  = [MMA]<sub>0</sub>/[1-PECl]<sub>0</sub> × M(MMA) × conversion.

Table S3 OMRP of styrene<sup>a</sup>

Entry	Complex	Conv. (%)	$M_{n,th [AIBN]}$ (Da)	$M_{n,th [Fe]}$ (Da)	$M_n$ (Da)	$\bar{D}$
S17	1a	45	2343	4686	8254	2.16
S18	2a	49	2552	5104	8294	2.27
S19	3a	35	1823	3646	6213	1.58
S20	4a	36	1875	3750	6561	1.61
S21	1b	43	2239	4478	8786	2.06
S22	3b	31	1614	3228	6881	1.86
S23	1c	41	2135	4270	8361	2.32
S24	3c	39	2031	4062	7104	1.92

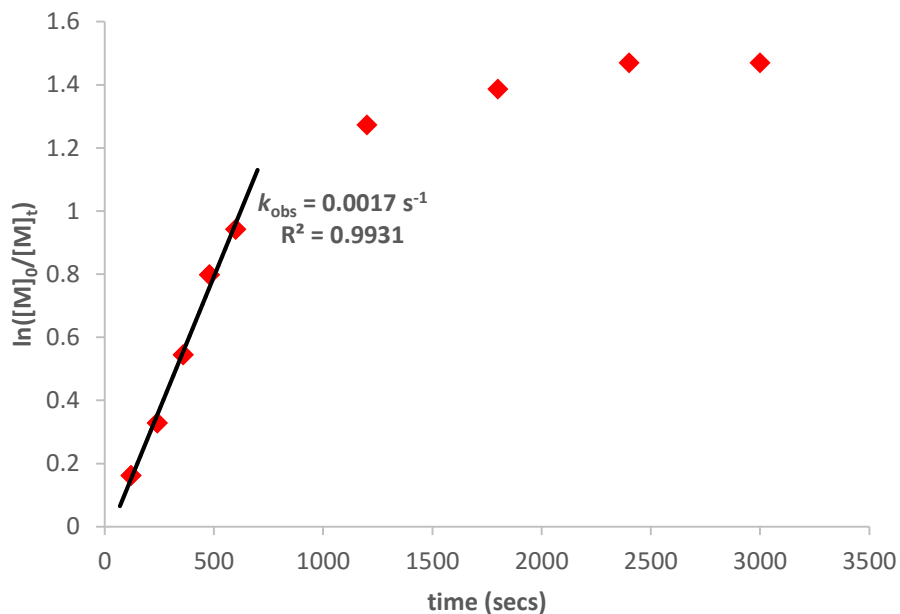
<sup>a</sup> Conditions: [styrene]:[Fe<sup>II</sup>]:[AIBN] = 100:1.00:1.00, styrene:toluene = 1:1 (v/v), 110°C, 1 hour. Conversion determined by <sup>1</sup>H NMR spectroscopy.  $M_{n,th [AIBN]} = [\text{styrene}]_0 / (2 \times [\text{AIBN}]_0) \times M(\text{styrene}) \times \text{conversion}$ .  $M_{n,th [Fe]} = [\text{styrene}]_0 / [\text{Fe}] \times M(\text{styrene}) \times \text{conversion}$ .

Table S4 OMRP of MMA<sup>a</sup>

Entry	Complex	Conv. (%)	$M_{n,th [AIBN]}$ (Da)	$M_{n,th [Fe]}$ (Da)	$M_n$ (Da)	$\bar{D}$
S25	1a	73	3654	7308	11764	1.47
S26	2a	69	3454	6908	11704	1.37
S27	3a	13	651	1302	13862	1.49
S28	4a	22	1101	2202	11128	1.53
S29	1b	56	2803	5606	10229	1.45
S30	3b	36	1802	3604	10123	1.41
S31	1c	54	2703	5406	10734	1.33
S32	3c	9	451	902	<sup>b</sup>	<sup>b</sup>

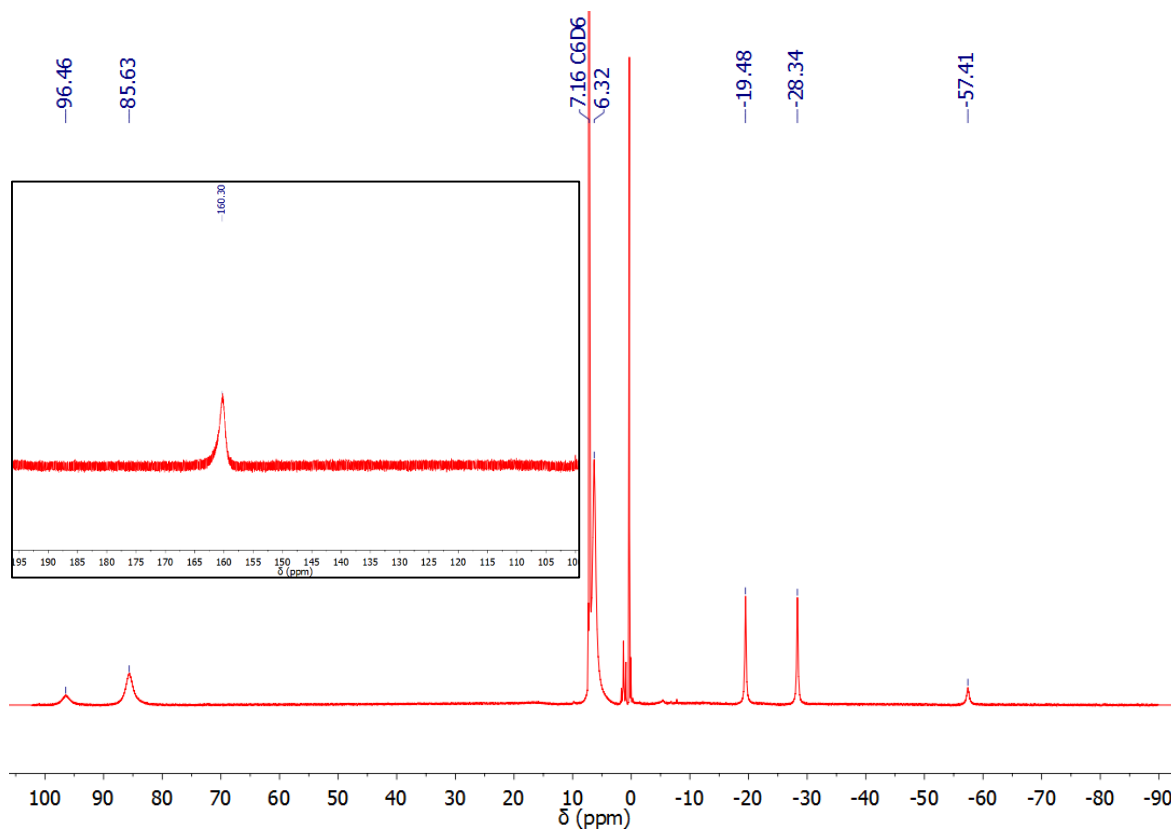
<sup>a</sup> Conditions: [MMA]:[Fe<sup>II</sup>]:[AIBN] = 100:1.00:1.00, MMA:toluene = 1:1 (v/v), 110°C, 1 hour. Conversion determined by <sup>1</sup>H NMR spectroscopy.  $M_{n,th [AIBN]} = [\text{MMA}]_0 / (2 \times [\text{AIBN}]_0) \times M(\text{MMA}) \times \text{conversion}$ .  $M_{n,th [Fe]} = [\text{MMA}]_0 / [\text{Fe}] \times M(\text{MMA}) \times \text{conversion}$ . <sup>b</sup> Too little polymer obtained for GPC analysis.

## KINETIC DATA

Figure S5 First-order kinetic plot for the OMRP of MMA mediated by complex **1a**<sup>a</sup>

<sup>a</sup> Conditions: [MMA]:[**1a**]:[AIBN] = 100:1.00:1.00, MMA:toluene = 1:1 (v/v), 110°C. Conversion determined by <sup>1</sup>H NMR spectroscopy.

## NMR SPECTRA

Figure S6 <sup>1</sup>H NMR spectrum of complex **1a** (500 MHz, C<sub>6</sub>D<sub>6</sub>)

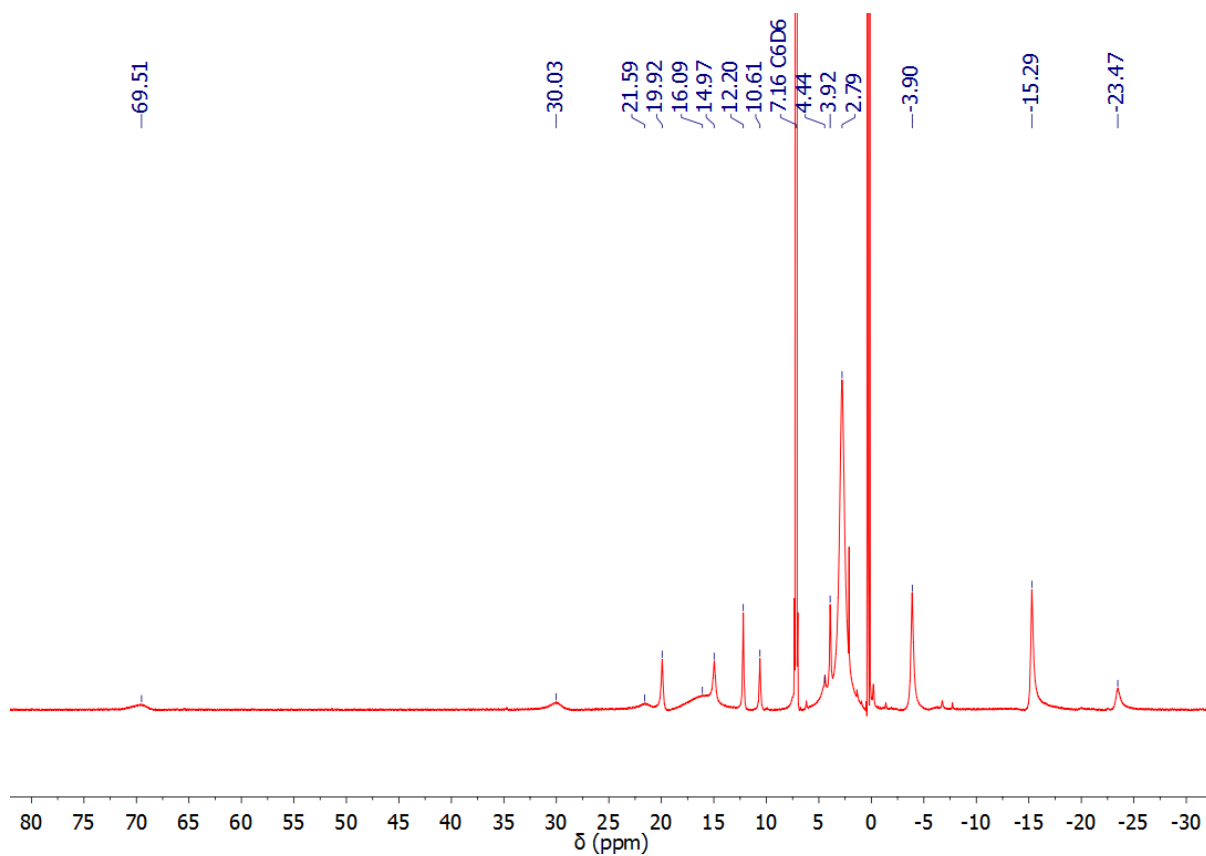
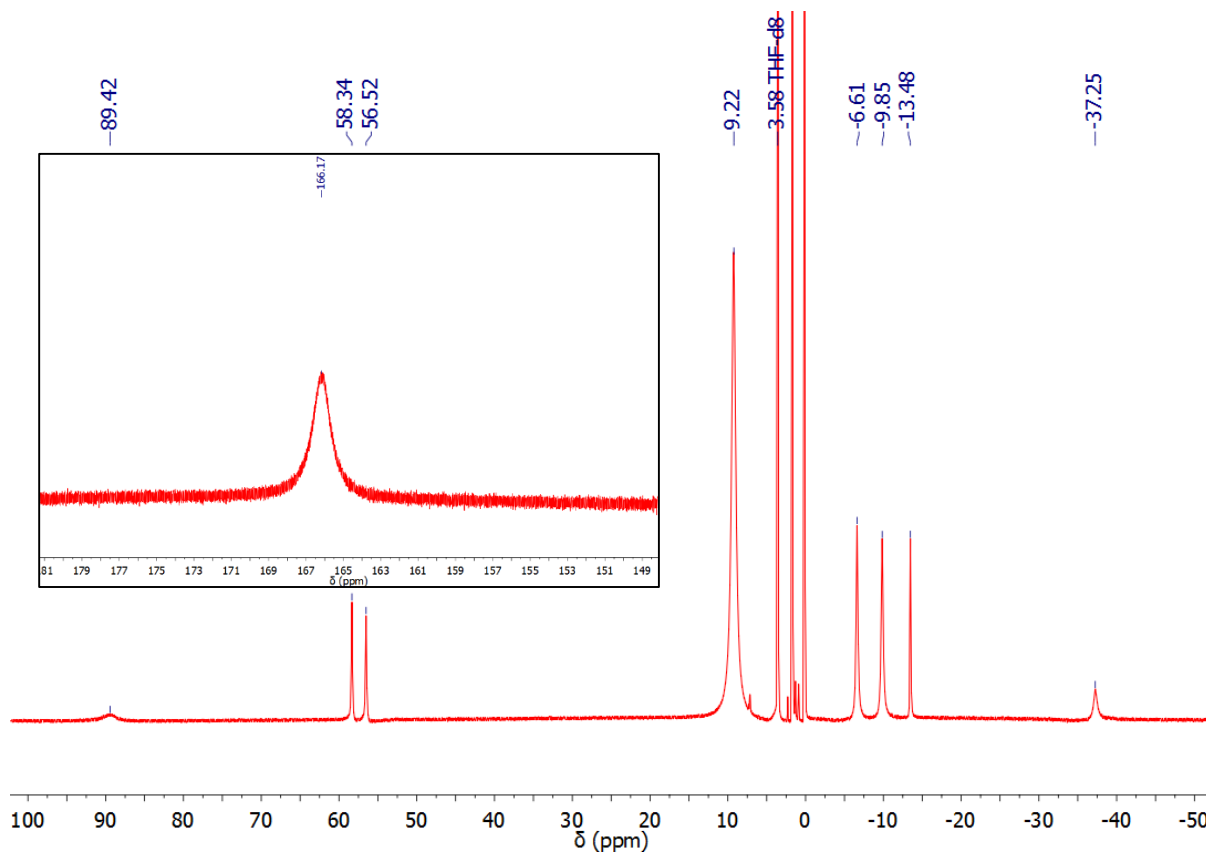
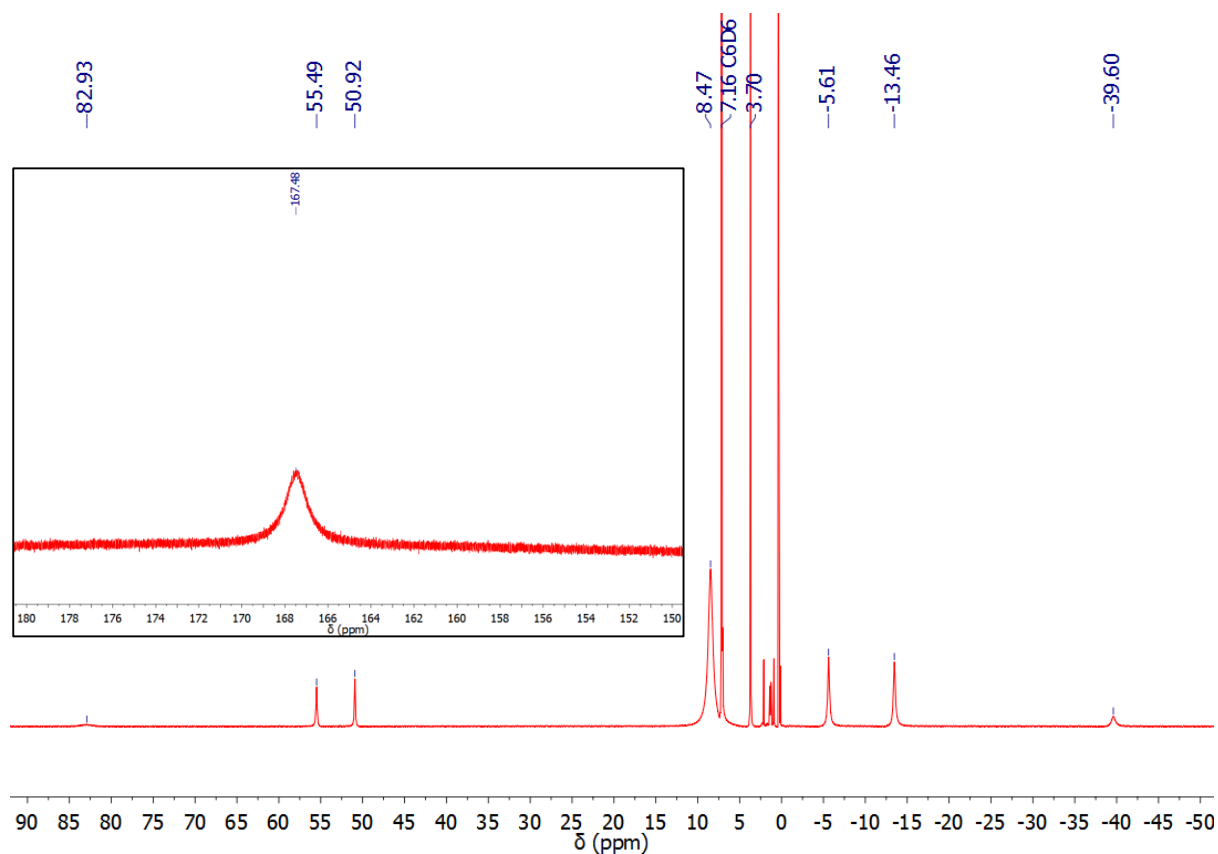
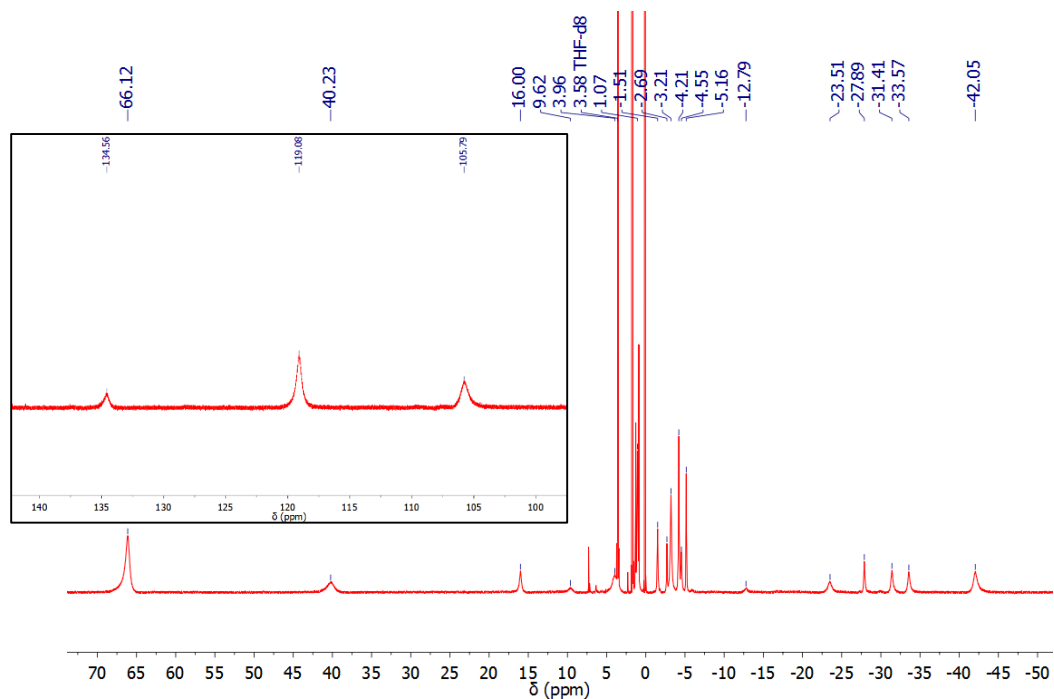
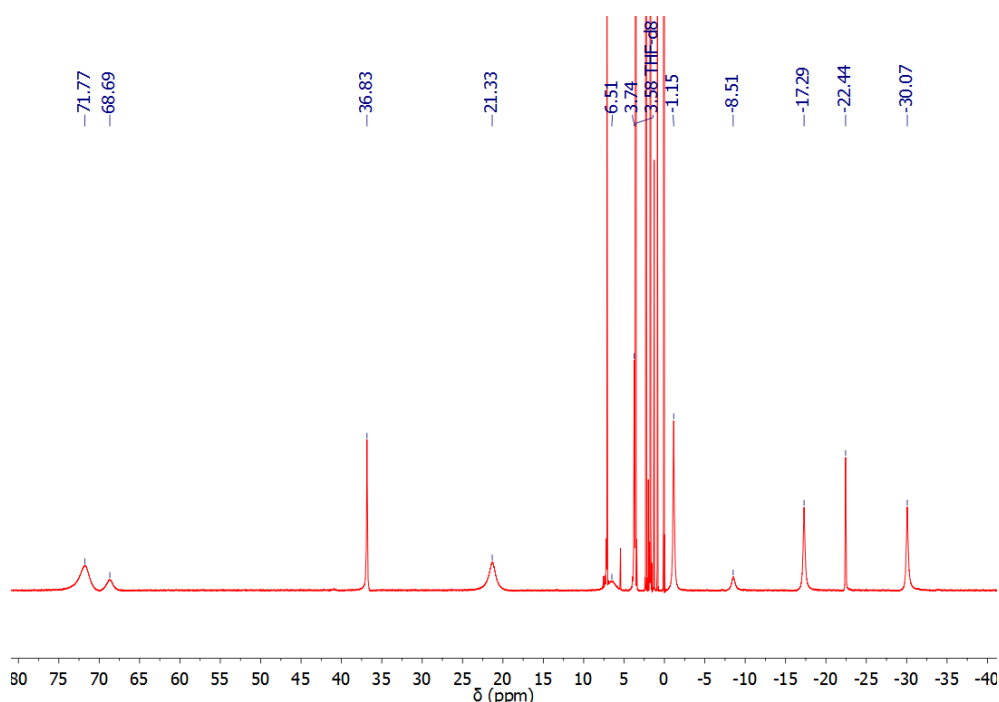
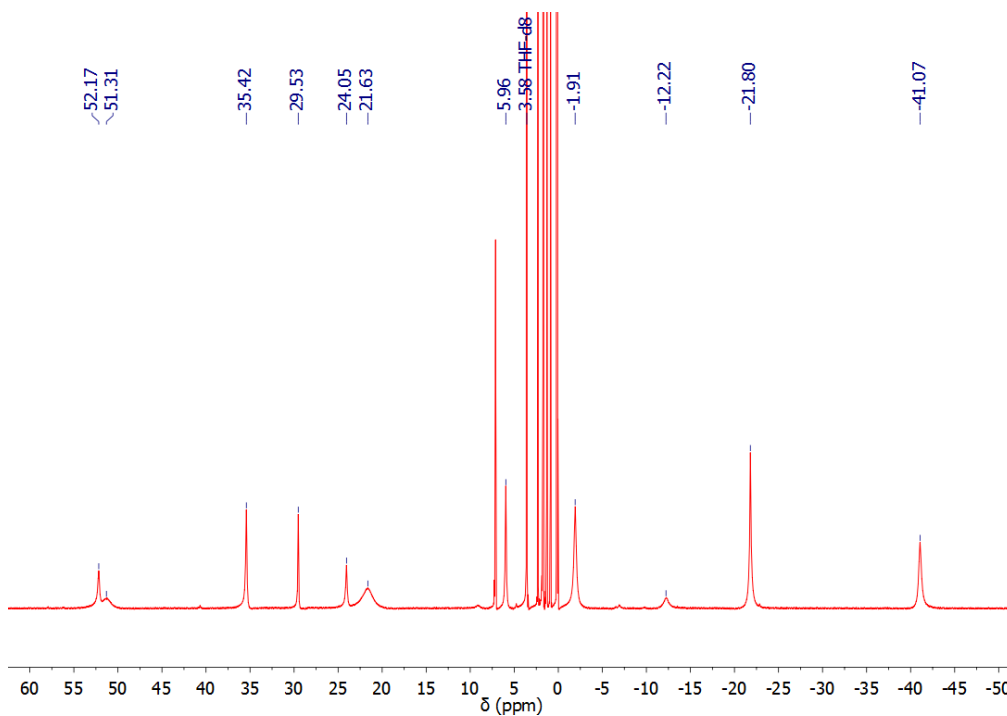
**Figure S7**  $^1\text{H}$  NMR spectrum of complex **2a** (500 MHz,  $\text{C}_6\text{D}_6$ )**Figure S8**  $^1\text{H}$  NMR spectrum of complex **3a** (500 MHz,  $\text{THF-d}_8$ )

Figure S9  $^1\text{H}$  NMR spectrum of complex **4a** (500 MHz,  $\text{C}_6\text{D}_6$ )Figure S10  $^1\text{H}$  NMR spectrum of complex **1b** (500 MHz,  $\text{THF-d}_8$ )

Note. The number of resonances observed in the  $^1\text{H}$  NMR spectrum of **1b** is double what would be expected based on the solid state structure. It is possible that multiple spectroscopically distinct species (e.g. monomers, dimers, etc.) are present in solution, thus giving rise to the higher than expected number of resonances. Combustion analysis and solution magnetic moment data together confirm the expected empirical formula of this complex.

**Figure S11**  $^1\text{H}$  NMR spectrum of complex **1c** (500 MHz,  $\text{THF-d}_8$ )

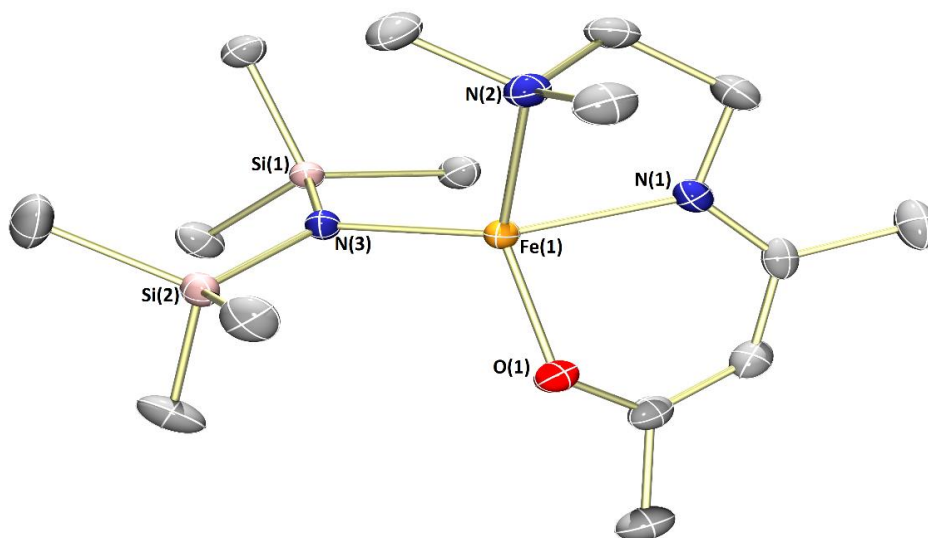
Note. A number of resonances corresponding to residual solvent (toluene and *n*-hexane) are apparent in the above spectrum, despite the spectrum being obtained from a 'dry' crystalline sample of complex **1c**. The appearance of residual solvent presumably arises through release of crystal lattice solvent on dissolution in  $\text{THF-d}_8$  (see **Figure S19** for x-ray structure).

**Figure S12**  $^1\text{H}$  NMR spectrum of complex **3c** (500 MHz,  $\text{THF-d}_8$ )

Note. A number of resonances corresponding to residual solvent (toluene and *n*-hexane) are apparent in the above spectrum, despite the spectrum being obtained from a 'dry' crystalline sample of complex **3c**. The appearance of residual solvent presumably arises through release of crystal lattice solvent on dissolution in  $\text{THF-d}_8$  (see **Figure S20** for x-ray structure).

## X-RAY CRYSTALLOGRAPHIC DATA

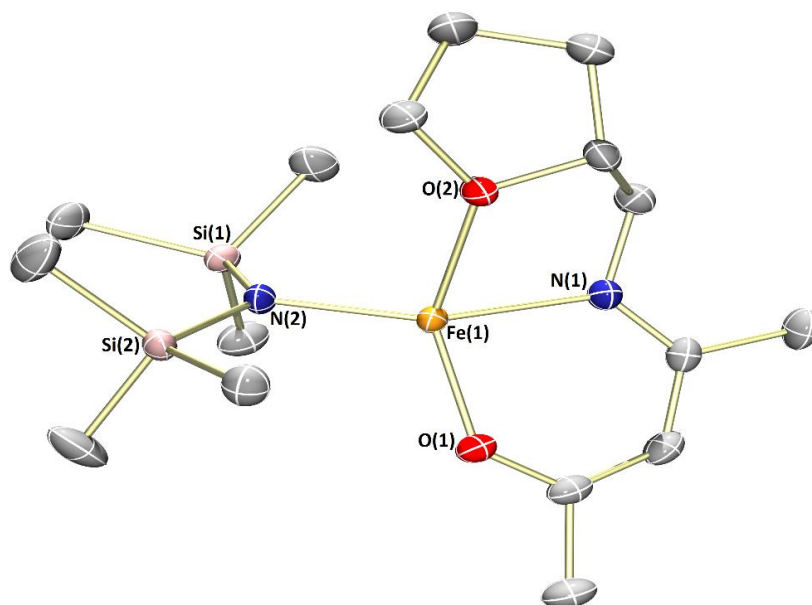
Figure S13 Complex 1a



CCDC Code	1470307	
Formula	$C_{15}H_{35}FeN_3OSi_2$	
Formula weight	385.49	
Size	0.3657 x 0.2421 x 0.125 mm	
Crystal morphology	Green block	
Temperature	119.97(18) K	
Wavelength	0.71073 Å [Mo- $K\alpha$ ]	
Crystal system	Monoclinic	
Space group	$P2_1/c$	
Unit cell dimensions	$a = 10.3546(6)$ Å	$\alpha = 90^\circ$
	$b = 15.0837(4)$ Å	$\beta = 127.970(9)^\circ$
	$c = 17.2714(10)$ Å	$\gamma = 90^\circ$
Volume	$2126.6(3)$ Å <sup>3</sup>	
Z	4	
Density (calculated)	1.204 Mg/m <sup>3</sup>	
Absorption coefficient	0.827 mm <sup>-1</sup>	
$F(000)$	832	
Data collection range	$2.837 \leq \theta \leq 31.076^\circ$	
Index ranges	$-14 \leq h \leq 14, -21 \leq k \leq 21, -24 \leq l \leq 23$	
Reflections collected	44800	
Independent reflections	6463 [ $R(\text{int}) = 0.0539$ ]	
Observed reflections	5349 [ $I > 2\sigma(I)$ ]	
Absorption correction	Gaussian	
Max. and min. transmission	0.975 and 0.95	

Refinement method	Full
Data / restraints / parameters	6463 / 0 / 209
Goodness of fit	1.055
Final <i>R</i> indices [ <i>I</i> > 2σ( <i>I</i> )]	<i>R</i> <sub>1</sub> = 0.0393, <i>wR</i> <sub>2</sub> = 0.0773
<i>R</i> indices (all data)	<i>R</i> <sub>1</sub> = 0.0537, <i>wR</i> <sub>2</sub> = 0.0826
Largest diff. peak and hole	0.4 and -0.261 e.Å <sup>-3</sup>

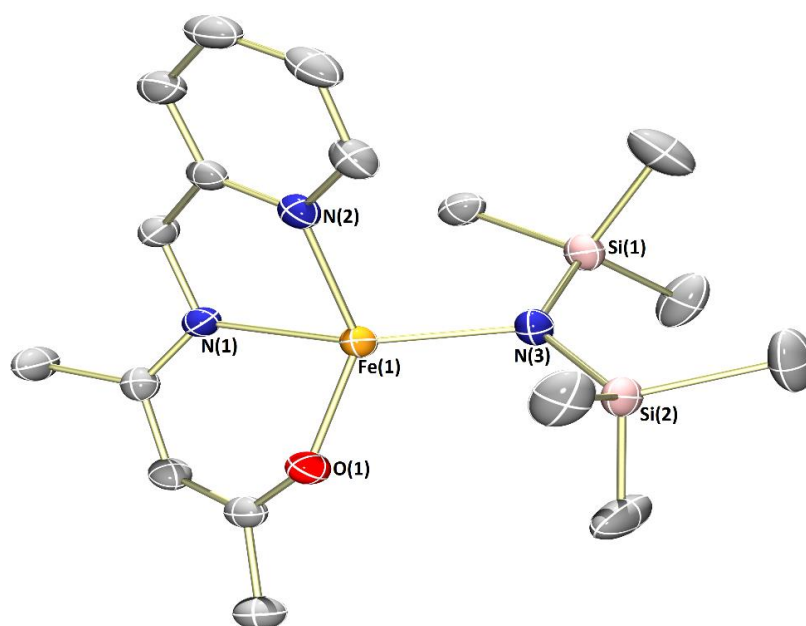
Figure S14 Complex 2a



CCDC Code	1470308	
Formula	C <sub>16</sub> H <sub>34</sub> FeN <sub>2</sub> O <sub>2</sub> Si <sub>2</sub>	
Formula weight	398.48	
Size	0.5458 x 0.4191 x 0.1544 mm	
Crystal morphology	Green plate	
Temperature	120.00(10) K	
Wavelength	0.71073 Å [Mo-K <sub>α</sub> ]	
Crystal system	Monoclinic	
Space group	<i>P</i> 2 <sub>1</sub> / <i>c</i>	
Unit cell dimensions	<i>a</i> = 12.06239(9) Å	<i>α</i> = 90°
	<i>b</i> = 9.46682(8) Å	<i>β</i> = 91.0690(7)°
	<i>c</i> = 18.89946(16) Å	<i>γ</i> = 90°
Volume	2157.80(3) Å <sup>3</sup>	
<i>Z</i>	4	
Density (calculated)	1.227 Mg/m <sup>3</sup>	
Absorption coefficient	0.819 mm <sup>-1</sup>	

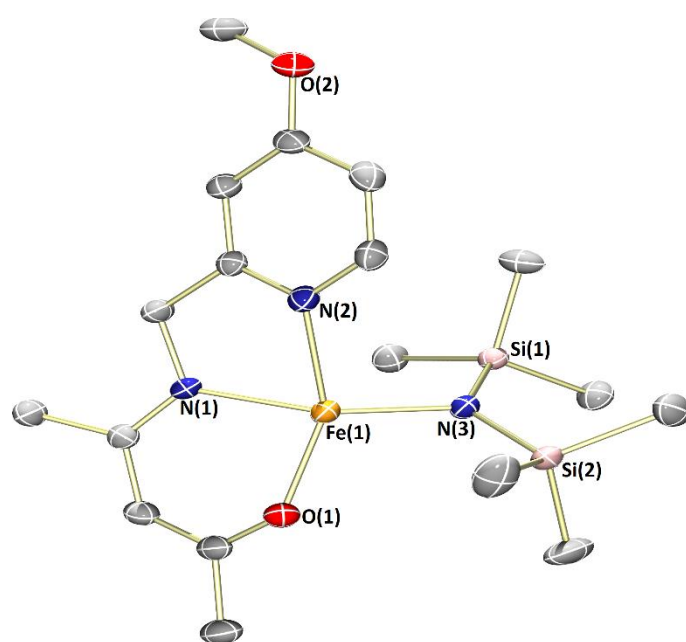
$F(000)$	856
Data collection range	$2.735 \leq \theta \leq 31.12^\circ$
Index ranges	$-17 \leq h \leq 17, -13 \leq k \leq 13, -26 \leq l \leq 27$
Reflections collected	44886
Independent reflections	6597 [ $R(\text{int}) = 0.0339$ ]
Observed reflections	5798 [ $I > 2\sigma(I)$ ]
Absorption correction	Gaussian
Max. and min. transmission	0.878 and 0.702
Refinement method	Full
Data / restraints / parameters	6597 / 0 / 216
Goodness of fit	1.074
Final $R$ indices [ $I > 2\sigma(I)$ ]	$R_1 = 0.0282, wR_2 = 0.0661$
$R$ indices (all data)	$R_1 = 0.035, wR_2 = 0.0697$
Largest diff. peak and hole	0.366 and $-0.232 \text{ e} \cdot \text{\AA}^{-3}$

Figure S15 Complex 3a



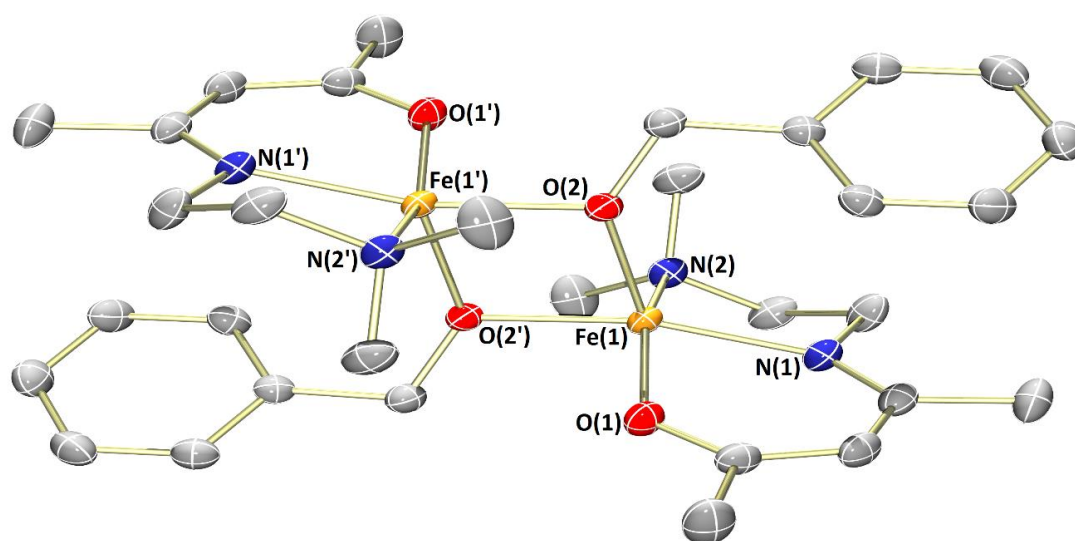
CCDC Code	1470309
Formula	$\text{C}_{17}\text{H}_{31}\text{FeN}_3\text{OSi}_2$
Formula weight	405.48
Size	0.4586 x 0.1651 x 0.109 mm
Crystal morphology	Intense green plate
Temperature	120.01(10) K
Wavelength	0.71073 Å [Mo- $K_\alpha$ ]
Crystal system	Monoclinic

Space group	$P2_1/c$	
Unit cell dimensions	$a = 15.8709(5) \text{ \AA}$	$\alpha = 90^\circ$
	$b = 16.3660(5) \text{ \AA}$	$\beta = 103.421(3)^\circ$
	$c = 8.6899(3) \text{ \AA}$	$\gamma = 90^\circ$
Volume	$2195.50(12) \text{ \AA}^3$	
Z	4	
Density (calculated)	$1.227 \text{ Mg/m}^3$	
Absorption coefficient	$0.805 \text{ mm}^{-1}$	
$F(000)$	864	
Data collection range	$2.712 \leq \theta \leq 29.665^\circ$	
Index ranges	$-21 \leq h \leq 21, -22 \leq k \leq 22, -12 \leq l \leq 10$	
Reflections collected	38643	
Independent reflections	5793 [ $R(\text{int}) = 0.0574$ ]	
Observed reflections	4655 [ $I > 2\sigma(I)$ ]	
Absorption correction	Gaussian	
Max. and min. transmission	0.977 and 0.905	
Refinement method	Full	
Data / restraints / parameters	5793 / 0 / 225	
Goodness of fit	1.063	
Final $R$ indices [ $I > 2\sigma(I)$ ]	$R_1 = 0.0434, wR_2 = 0.0845$	
$R$ indices (all data)	$R_1 = 0.0615, wR_2 = 0.0915$	
Largest diff. peak and hole	$0.435$ and $-0.311 \text{ e. \AA}^{-3}$	

**Figure S16** Complex 4a

CCDC Code	1470310	
Formula	$C_{18}H_{33}FeN_3O_2Si_2$	
Formula weight	435.5	
Size	0.4065 x 0.174 x 0.1573 mm	
Crystal morphology	Green block	
Temperature	120.00(10) K	
Wavelength	0.71073 Å [Mo- $K\alpha$ ]	
Crystal system	Triclinic	
Space group	<i>P</i> -1	
Unit cell dimensions	$a = 8.8657(6)$ Å	$\alpha = 90.425(4)^\circ$
	$b = 10.8724(6)$ Å	$\beta = 100.153(5)^\circ$
	$c = 12.2568(5)$ Å	$\gamma = 97.601(5)^\circ$
Volume	1152.16(11) Å <sup>3</sup>	
<i>Z</i>	2	
Density (calculated)	1.255 Mg/m <sup>3</sup>	
Absorption coefficient	0.774 mm <sup>-1</sup>	
<i>F</i> (000)	464	
Data collection range	$2.814 \leq \theta \leq 31.03^\circ$	
Index ranges	$-12 \leq h \leq 11$ , $-15 \leq k \leq 14$ , $-17 \leq l \leq 17$	
Reflections collected	24682	
Independent reflections	6749 [ <i>R</i> (int) = 0.0535]	
Observed reflections	5501 [ <i>I</i> > 2σ( <i>I</i> )]	
Absorption correction	Gaussian	
Max. and min. transmission	0.952 and 0.905	
Refinement method	Full	
Data / restraints / parameters	6749 / 0 / 244	
Goodness of fit	1.06	
Final <i>R</i> indices [ <i>I</i> > 2σ( <i>I</i> )]	$R_1 = 0.0428$ , $wR_2 = 0.0996$	
<i>R</i> indices (all data)	$R_1 = 0.0555$ , $wR_2 = 0.1088$	
Largest diff. peak and hole	0.715 and -0.491 e.Å <sup>-3</sup>	

Figure S17 Complex 1b

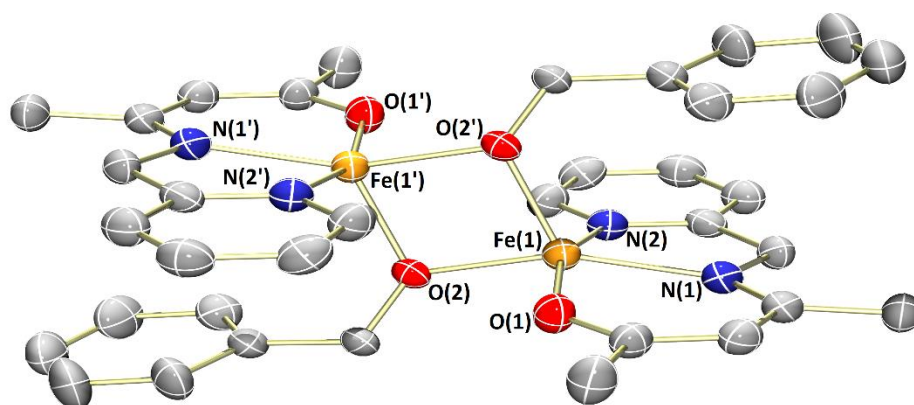


CCDC Code	1470323	
Formula	$C_{32}H_{48}Fe_2N_4O_4$	
Formula weight	664.44	
Size	0.6512 x 0.1049 x 0.1016 mm	
Crystal morphology	Orange plate	
Temperature	120.00(10) K	
Wavelength	0.71073 Å [Mo- $K_{\alpha}$ ]	
Crystal system	Triclinic	
Space group	$P-1$	
Unit cell dimensions	$a = 7.8337(3)$ Å	$\alpha = 84.382(3)^{\circ}$
	$b = 10.2379(3)$ Å	$\beta = 72.596(4)^{\circ}$
	$c = 10.7448(4)$ Å	$\gamma = 86.906(3)^{\circ}$
Volume	$818.06(6)$ Å <sup>3</sup>	
Z	1	
Density (calculated)	1.349 Mg/m <sup>3</sup>	
Absorption coefficient	0.927 mm <sup>-1</sup>	
$F(000)$	352	
Data collection range	$2.862 \leq \theta \leq 31.142^{\circ}$	
Index ranges	$-11 \leq h \leq 10, -14 \leq k \leq 14, -15 \leq l \leq 15$	
Reflections collected	35409	
Independent reflections	4970 [ $R(\text{int}) = 0.0382$ ]	
Observed reflections	4603 [ $I > 2\sigma(I)$ ]	
Absorption correction	Gaussian	
Max. and min. transmission	0.926 and 0.709	
Refinement method	Full	

Data / restraints / parameters	4970 / 0 / 194
Goodness of fit	1.086
Final <i>R</i> indices [ <i>I</i> > 2σ( <i>I</i> )]	<i>R</i> <sub>1</sub> = 0.0318, <i>wR</i> <sub>2</sub> = 0.0707
<i>R</i> indices (all data)	<i>R</i> <sub>1</sub> = 0.0359, <i>wR</i> <sub>2</sub> = 0.0723
Largest diff. peak and hole	0.494 and -0.284 e.Å <sup>-3</sup>

**Figure S18** Complex **3b**

*Note.* Crystals of complex **3b** were generally observed to be of very poor quality. However, a suitable single crystal was eventually found and a data set obtained. The asymmetric unit of complex **3b** was found to contain two crystallographically-distinct [Fe(L)OBn] units, with each representing half of a (μ<sup>2</sup>-OBn)<sub>2</sub> bridged dimer. The two halves of each dimer are crystallographically related through inversion. After some preliminary structural refinement, a very large residual electron density peak was observed in the vicinity of Fe2, along with further, more diffuse electron density. Therefore, the [Fe(L)OBn] unit initially containing Fe2 was modelled as being split over two positions with SOFs of 0.75 for the major component (containing Fe2A) and 0.25 for the minor component (containing Fe2B). One of the β-ketiminate methyl groups (C23) was best modelled as being common to both disorder components. Unfortunately, the OBn group of the minor disorder component appeared disordered further, and could not be satisfactorily refined without the use of EADP constraints. Therefore, this group was refined isotropically. The disordered nature of this structure accounts for the large number of checkCIF alerts.

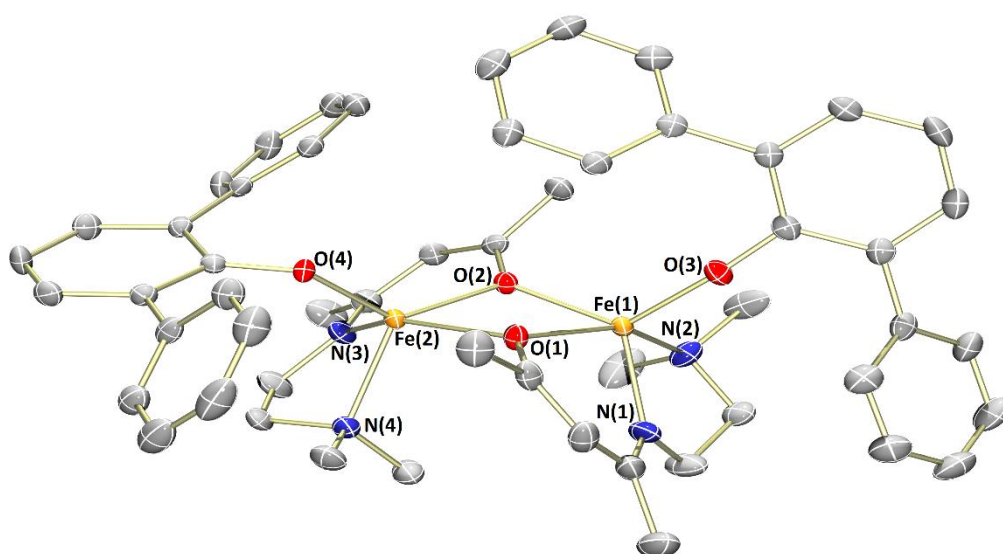


CCDC Code	1470324	
Formula	C <sub>36</sub> H <sub>40</sub> Fe <sub>2</sub> N <sub>4</sub> O <sub>4</sub>	
Formula weight	704.42	
Size	0.1677 x 0.1112 x 0.0678 mm	
Crystal morphology	Dark red plate	
Temperature	120.00(10) K	
Wavelength	1.54184 Å [Cu-Kα]	
Crystal system	Monoclinic	
Space group	P2 <sub>1</sub> /c	
Unit cell dimensions	<i>a</i> = 8.2528(4) Å	<i>α</i> = 90°
	<i>b</i> = 18.5226(6) Å	<i>β</i> = 119.539(7)°
	<i>c</i> = 24.7956(13) Å	<i>γ</i> = 90°
Volume	3297.7(3) Å <sup>3</sup>	

Z	4
Density (calculated)	1.419 Mg/m <sup>3</sup>
Absorption coefficient	7.42 mm <sup>-1</sup>
F(000)	1472
Data collection range	3.145 ≤ θ ≤ 76.889°
Index ranges	-6 ≤ h ≤ 10, -23 ≤ k ≤ 23, -31 ≤ l ≤ 30
Reflections collected	53543
Independent reflections	6864 [R(int) = 0.1062]
Observed reflections	5515 [I > 2σ(I)]
Absorption correction	multi-scan
Max. and min. transmission	1 and 0.54604
Refinement method	Full
Data / restraints / parameters	6864 / 5 / 553
Goodness of fit	1.2
Final R indices [I > 2σ(I)]	R <sub>1</sub> = 0.0861, wR <sub>2</sub> = 0.1848
R indices (all data)	R <sub>1</sub> = 0.102, wR <sub>2</sub> = 0.1922
Largest diff. peak and hole	0.689 and -0.506 e.Å <sup>-3</sup>

**Figure S19** Complex **1c**

*Note. The asymmetric unit of complex 1c was found to consist of two structurally analogous dimers (only one shown below), and two regions of co-crystallised solvent. One region could be easily modelled as a molecule of toluene with an SOF of 1. The contents of the additional solvent region were a little less clear, though could be modelled as containing either one molecule of toluene (SOF = 0.66) or one molecule of hexane (SOF = 0.33) (this explains the non-integer value in the chemical formula shown below). A number of geometric and ADP constraints/restraints were required to generate chemically sensible structures of the disordered solvent.*

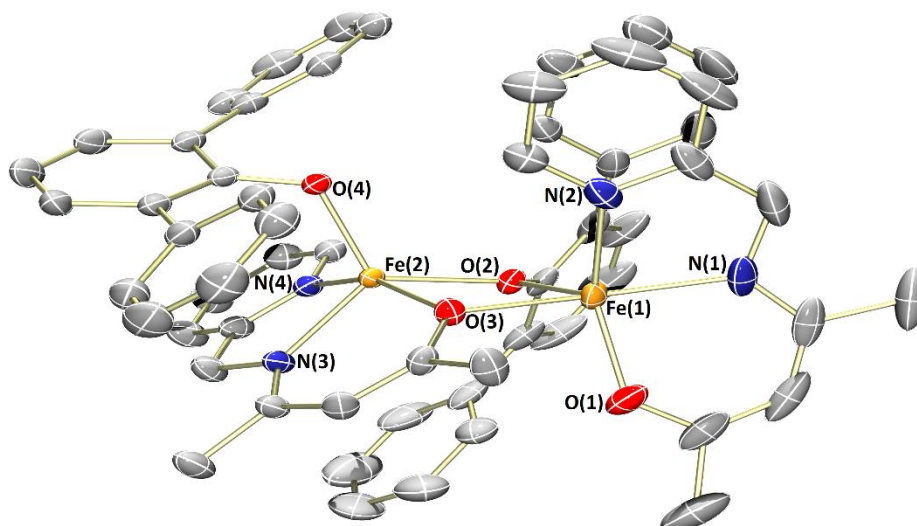


CCDC Code	1470383
Formula	C <sub>60.83</sub> H <sub>69</sub> Fe <sub>2</sub> N <sub>4</sub> O <sub>4</sub>

Formula weight	1031.9	
Size	0.47 x 0.27 x 0.06 mm	
Crystal morphology	Orange plate	
Temperature	120.00(10) K	
Wavelength	0.71073 Å [Mo-K $\alpha$ ]	
Crystal system	Monoclinic	
Space group	$P2_1/c$	
Unit cell dimensions	$a = 34.0413(13)$ Å	$\alpha = 90^\circ$
	$b = 15.5968(6)$ Å	$\beta = 98.031(3)^\circ$
	$c = 20.4395(7)$ Å	$\gamma = 90^\circ$
Volume	10745.7(7) Å <sup>3</sup>	
Z	8	
Density (calculated)	1.276 Mg/m <sup>3</sup>	
Absorption coefficient	0.59 mm <sup>-1</sup>	
$F(000)$	4368	
Data collection range	$2.747 \leq \theta \leq 25.351^\circ$	
Index ranges	$-41 \leq h \leq 40, -18 \leq k \leq 18, -24 \leq l \leq 23$	
Reflections collected	157681	
Independent reflections	19635 [ $R(\text{int}) = 0.0987$ ]	
Observed reflections	15942 [ $I > 2\sigma(I)$ ]	
Absorption correction	Gaussian	
Max. and min. transmission	0.998 and 0.99	
Refinement method	Full	
Data / restraints / parameters	19635 / 17 / 1311	
Goodness of fit	1.121	
Final $R$ indices [ $I > 2\sigma(I)$ ]	$R_1 = 0.0608, wR_2 = 0.1085$	
$R$ indices (all data)	$R_1 = 0.0819, wR_2 = 0.1158$	
Largest diff. peak and hole	0.747 and -0.487 e.Å <sup>-3</sup>	

### Figure S20 Complex 3c

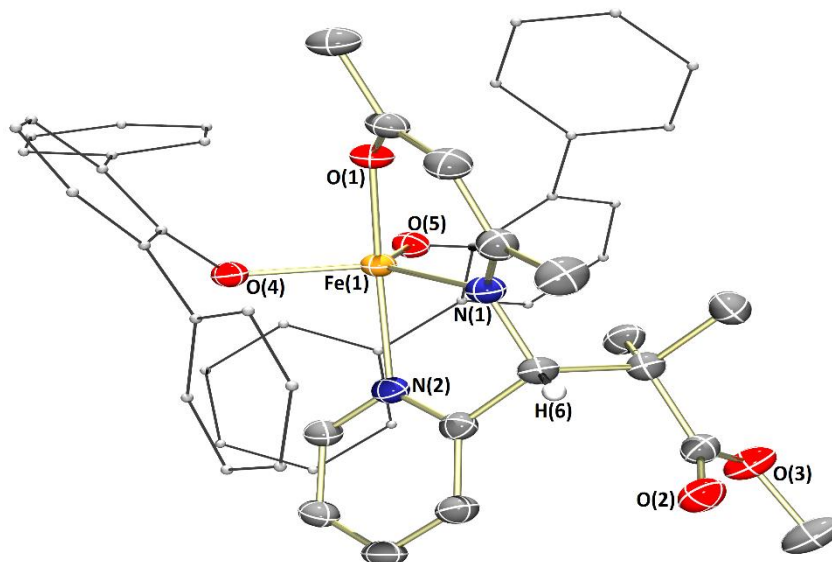
*Note. Regions of diffuse, poorly resolved electron density were observed in the crystalline lattice, but could not be modelled satisfactorily as solvent (toluene or hexane). This residual electron density was removed using the SQUEEZE routine in PLATON. In all, electron density (125 electrons) pertaining to 2.5 molecules of toluene (or hexane) per unit cell was removed. This is included in the chemical formula and as a result produces many errors in checkCIF which should be ignored.*



CCDC Code	1470384	
Formula	$C_{62.38}H_{57}Fe_2N_4O_4$	
Formula weight	1038.32	
Size	0.3462 x 0.2548 x 0.0594 mm	
Crystal morphology	Orange block	
Temperature	120.00(10) K	
Wavelength	0.71073 Å [Mo- $K\alpha$ ]	
Crystal system	Monoclinic	
Space group	$P2_1/c$	
Unit cell dimensions	$a = 12.7953(2)$ Å	$\alpha = 90^\circ$
	$b = 14.0417(3)$ Å	$\beta = 91.2680(17)^\circ$
	$c = 30.0899(6)$ Å	$\gamma = 90^\circ$
Volume	$5404.83(18)$ Å <sup>3</sup>	
Z	4	
Density (calculated)	1.276 Mg/m <sup>3</sup>	
Absorption coefficient	0.588 mm <sup>-1</sup>	
$F(000)$	2173	
Data collection range	$2.937 \leq \theta \leq 28.281^\circ$	
Index ranges	$-17 \leq h \leq 17, -18 \leq k \leq 18, -40 \leq l \leq 40$	
Reflections collected	140618	
Independent reflections	13322 [ $R(\text{int}) = 0.0579$ ]	
Observed reflections	11966 [ $I > 2\sigma(I)$ ]	
Absorption correction	Multi-scan	
Max. and min. transmission	1 and 0.89445	
Refinement method	Full	
Data / restraints / parameters	13322 / 0 / 617	

Goodness of fit	1.191
Final <i>R</i> indices [ <i>I</i> > 2σ( <i>I</i> )]	<i>R</i> <sub>1</sub> = 0.0749, <i>wR</i> <sub>2</sub> = 0.1619
<i>R</i> indices (all data)	<i>R</i> <sub>1</sub> = 0.086, <i>wR</i> <sub>2</sub> = 0.1672
Largest diff. peak and hole	0.794 and -0.641 e.Å <sup>-3</sup>

Figure S21 Complex 3c'



CCDC Code	1470385	
Formula	C <sub>52</sub> H <sub>47</sub> FeN <sub>2</sub> O <sub>5</sub>	
Formula weight	835.76	
Size	0.1631 x 0.113 x 0.0591 mm	
Crystal morphology	Black fragment	
Temperature	120.00(10) K	
Wavelength	1.54184 Å [Cu-K <sub>α</sub> ]	
Crystal system	Triclinic	
Space group	<i>P</i> -1	
Unit cell dimensions	<i>a</i> = 11.8082(3) Å	<i>α</i> = 84.253(2)°
	<i>b</i> = 12.0560(4) Å	<i>β</i> = 75.270(2)°
	<i>c</i> = 15.9552(4) Å	<i>γ</i> = 75.487(2)°
Volume	2125.01(11) Å <sup>3</sup>	
<i>Z</i>	2	
Density (calculated)	1.306 Mg/m <sup>3</sup>	
Absorption coefficient	3.254 mm <sup>-1</sup>	
<i>F</i> (000)	878	
Data collection range	3.79 ≤ <i>θ</i> ≤ 76.13°	
Index ranges	-14 ≤ <i>h</i> ≤ 14, -15 ≤ <i>k</i> ≤ 15, -20 ≤ <i>l</i> ≤ 19	
Reflections collected	52301	

Independent reflections	8832 [ $R(\text{int}) = 0.0691$ ]
Observed reflections	8288 [ $I > 2\sigma(I)$ ]
Absorption correction	multi-scan
Max. and min. transmission	1 and 0.77371
Refinement method	Full
Data / restraints / parameters	8832 / 0 / 546
Goodness of fit	1.046
Final $R$ indices [ $I > 2\sigma(I)$ ]	$R_1 = 0.0471$ , $wR_2 = 0.1214$
$R$ indices (all data)	$R_1 = 0.0498$ , $wR_2 = 0.1251$
Largest diff. peak and hole	0.624 and $-0.916\text{e}\cdot\text{\AA}^{-3}$